Re-Os systematics and age of pyrite associated with stratiform Zn-Pb mineralization in the Howards Pass district, Yukon and Northwest Territories, Canada

Karen D. Kelley[1], David Selby[2], Hendrik Falck[3], and John F. Slack[4]

[1]U.S. Geological Survey, MS 973, Denver, CO 80225 USA; kdkelley@usgs.gov

[2]Department of Earth Sciences, University of Durham, Durham, DH1 3LE UK

[3] NWT Geoscience Office, P.O. Box 1320, Yellowknife, NWT X1A 2L9 Canada

[4]U.S. Geological Survey (Emeritus), MS 954, Reston, VA 20192 USA

Abstract

Stratiform Zn-Pb deposits hosted in unmetamorphosed carbonaceous and siliceous mudstones of the Ordovician to Silurian Duo Lake Formation define the Howards Pass district in Yukon Territory and Northwest Territories, western Canada. Collectively, the deposits are among the largest in the world, containing drill-indicated and inferred resources of 423 Mt at 4.84% Zn and 1.59% Pb. Sulphide textures include: (a) fine-scale laminations of sphalerite, galena, and pyrite from <0.05 mm to 1 cm thick, interbedded with carbonaceous sedimentary rock; (b) layers of coarse sulphide that are structurally controlled by microfolds; and (c) veins that cut bedding and sulphide laminations. The finely interlaminated nature of sulphides with mudstone has been used as evidence for syngenetic mineralizing processes, whereas paleomagnetic data determined on coarse layered sulphides suggest a Middle Jurassic age of mineralization.

Here, we present new Re-Os isotopic data for 12 pyrite separates obtained from 4 laminated sulphide-rich samples from the XY Central (XYC) and Don (DON) deposits, and for 1 unmineralized organic-rich mudstone ~20 m stratigraphically below the sulphide-bearing zone. Pyrite separates that lack mudstone inclusions ("pure") from the XYC deposit contain 2.2 to 4.0 ppb Re, and 93.4 to 123.4 ppt Os; pure pyrite from the DON deposit is significantly more enriched in Re and Os (34–37 ppb Re; 636.8–694.9 ppt

Os). The $^{187}Re/^{188}Os$ values of pure pyrite separates from the XYC and DON deposits range from 137.6 to 197 and 182.1 to 201.4, respectively. Regression of all pure pyrite Re-Os data from both deposits yields an isochron age of 442 ± 14 Ma (MSWD = 7.4) and an initial $^{187}Os/^{188}Os$ (Os_i) value of 0.71 ± 0.07. The Re-Os age indicates that the early phase of pyrite precipitation (and by inference, sphalerite and galena) occurred during the early Silurian, consistent with biostratigraphic ages of the host rocks. The Os_i value of ~0.8 for earliest Silurian seawater recorded from organic-rich shale in the basal Silurian Global Stratotype Section and Point (GSSP) at Dobs Linn, Scotland, is very similar to that provided by the Howards Pass pyrite regression, and hence suggests a hydrogenous (seawater) source of Os for the pyrite. Therefore, two possible sources of Os are (1) the Zn- and Pb-bearing hydrothermal fluid that leached Os from footwall sedimentary rocks, which were deposited in seawater; or (2) directly from seawater during precipitation of the pyrite, which suggests that the Os content of the hydrothermal fluid was minor relative to that of seawater.

Keywords: Re-Os isotopes, geochronology, Howards Pass, stratabound Zn-Pb, Yukon Territory, Northwest Territories

Introduction

The Zn-Pb deposits of the Howards Pass district occur in lower Paleozoic strata of the Selwyn Basin in the northern Canadian Cordillera, primarily in eastern Yukon Territory, but extending across the border into Northwest Territories (Fig. 1). Other Zn-Pb districts in the Selwyn Basin include Macmillan Pass or “MacPass” (Tom and Jason deposits), Anvil (Faro, Grum, Swim, Vangorda, and Dy deposits), and Gataga (Cirque and Driftpile deposits).

In the Howards Pass district, at least 15 mineralized zones have been identified over a strike length of ~38 km (Fig. 2) (Selwyn Chihong Mining Ltd., 2016). Mineralized zones consist of finely laminated to layered sulphides, or coarse sulphides occurring in veins, foliations, thin fractures, and cleavage planes that cut the laminations and layers. Sulphide minerals include sphalerite, galena, and minor pyrite; chalcopyrite is rare. Collectively, the Zn-Pb deposits are among the largest in the world (Goodfellow 2004; Leach et al. 2005), in total containing 423 Mt of drill-indicated and inferred resources at an average grade of 4.84% Zn and 1.59 % Pb (Kirkham et al. 2012).

The deposits in the Howards Pass district are classified as clastic-dominated lead-zinc (CD Zn-Pb) ores, which are typically hosted in shale, sandstone, siltstone, or mixed clastic lithologies, or form replacements of carbonate rocks within a clastic-dominated sedimentary sequence (Leach et al. 2010). CD Zn-Pb deposits are stratabound and mostly stratiform, and commonly display laminated sulphide textures; therefore, they are assumed to have formed synchronously with sedimentation and/or during early burial and diagenesis. However, intricately interlayered sulphides can also be produced by replacement that mimics primary sedimentary features (e.g., Kelley et al. 2004a; Leach et al. 2005). In addition, original textures can be modified by post-mineralization deformation and recrystallization.

Textural and paleomagnetic data for the deposit offer contrasting temporal relationships between sedimentation and mineralization in the Howards Pass district. Although not definitive, the finely laminated nature of sulphides intergrown with mudstone has been used as evidence for syngenetic or syndiagenetic mineralizing processes during the early Silurian, given conodont and graptolite biostratigraphic data

for the host rocks (Morganti 1979; Norford and Orchard 1985; Goodfellow and Jonasson 1986). Crosscutting textures may record recrystallization of primary, fine-grained sulphides by pressure dissolution during synsedimentary deformation (Jonasson and Goodfellow 1986). An alternative explanation is that the laminated sulphides formed concurrently with abundant, secondary, coarse-grained sulphide minerals that occur along cleavage planes and in thin fractures throughout the deposits. The northeast dip of the cleavage planes and their alignment with northwest-trending regional folds (Gordey and Anderson 1993; Martel 2015) suggest that the coarse-grained sulphides formed during tectonism, the onset of which regionally occurred in the Jurassic to Cretaceous (Dusel-Bacon et al. 2002; Mair et al. 2006). Furthermore, paleomagnetic dating of coarse-grained sulphide veins in the Howards Pass district indicate that they formed during the Middle Jurassic, leading to the further suggestion that the fine-grained sulphides may also have formed at this time (Kawasaki and Symons 2012). Establishing with certainty the age of the laminated sulphide minerals is therefore critical for developing a robust genetic model for the Howards Pass deposits. If the laminated sulphides indeed formed during the Mesozoic, then a tectonically related genesis must be invoked that is distinct from the synsedimentary to syndiagenetic model that is predominant for CD Zn-Pb deposits (see Leach et al. 2010).

Documenting the timing of mineralization for CD Zn-Pb deposits has traditionally been difficult owing mainly to a lack of datable minerals within the deposits. Commonly, global Pb-isotope growth curves are used to calculate model Pb ages for CD Zn-Pb deposits. However, many ages obtained by this approach are much older than their respective host rocks, and therefore such global growth curves should not be used to

calculate model Pb ages (Leach et al. 2005). A better approach involves the application of terrane-specific Pb growth curves, as was done for deposits in northern Australia (Large et al. 2005) and the Selwyn Basin (Godwin and Sinclair 1982). However, the underlying assumption in building these curves is that mineralization formed by syngenetic processes. If the deposits to be dated formed after deposition of the host rocks, then such Pb-isotope growth curves are not relevant for dating mineralization.

The recent application of the rhenium-osmium (Re-Os) chronometer to Fe- and Cu-bearing sulphide minerals has demonstrated the feasibility of directly dating ore mineralization. However, Red Dog is the only CD Zn-Pb deposit that has been dated successfully by Re-Os methods, due in part to the coarse-grained nature of the sulphide minerals there and to the relatively high Re contents (tens to hundreds of parts per billion) of pyrite within the vein and massive ore (Morelli et al. 2004). Base-metal sulphides in other types of sediment-hosted deposits have also been directly dated using Re-Os geochronology, including the Lince-Estefanía Cu deposit in northern Chile (Tristá-Aguilera et al. 2006), the Kipushi Cu-Co deposit in the Democratic Republic of Congo (Schneider et al. 2007), the Ruby Creek Cu-Co deposit in Alaska (Selby et al. 2009), the Tuolugou Co-Au deposit in northwestern China (Feng et al. 2009), the Lisheen and Silvermines Zn-Pb deposits in Ireland (Hnatyshin et al. 2015), and the Caixiashan deposit in northwestern China (Li et al. 2016).

This paper presents new Re-Os data for pyrite and black shale from the XY Central (XYC) and DON deposits in the Howards Pass district (Fig. 2). The Re-Os results presented herein (1) further demonstrate the utility of using sulphide minerals for geochronology, (2) deepen our understanding of Re-Os systematics in CD Zn-Pb

deposits, (3) document an age for the layered and laminated stage of mineralization, and (4) provide implications for the origin of the metals.

Regional and local geology

Stratiform CD Zn-Pb deposits are common in the Selwyn Basin of western Canada. This basin formed by passive margin sedimentation from the Neoproterozoic to Devonian. Underlying strata of the Selwyn Basin are Mesoproterozoic and older crystalline rocks overlain by Mesoproterozoic metasedimentary rocks and mafic sills related to rift sedimentation and crustal extension that is bracketed between 1.59 and 1.38 Ga (Eisbacher 1985; Snyder et al. 2009).

The passive margin sequence within the Selwyn Basin consists of two northwest-trending belts of rocks (Gordey and Anderson 1993): (1) in the northeast, the Mackenzie Platform comprises Neoproterozoic to Middle Devonian shallow-water carbonate and sandstone; (2) in the southwest, sedimentary strata include time-equivalent siliciclastic rocks (Neoproterozoic Windermere Supergroup), deep-water limestone (Cambrian Rabbitkettle Formation), and shale and chert of the Ordovician to Silurian Road River Group. Passive margin sedimentation was punctuated by periods of extension and tectonic instability. Mafic igneous rocks occur locally in the Selwyn Basin (Fig. 1) as a result of middle to late Cambrian and Middle Ordovician volcanism (Goodfellow et al. 1995).

Devonian-Mississippian black shale, chert, and clastic units of the Earn Group overlie the Road River Group (Fig. 3) (Morganti 1979; Gordey 1980). Deposition of

rocks in the Earn Group reflects regional uplift and erosion followed by subsidence of the continental margin.

Regionally developed Early to Middle Cretaceous compression and deformation occurred during eastward docking of allochthonous terranes against the North American continent (Gordey and Anderson 1993; Mair et al. 2006). This Cretaceous tectonism in the Howards Pass district resulted in the formation of thin-skinned detachments, folds, imbricate thrusts, and duplex structures (Hodder et al. 2014; Martel 2015); in contrast, large-scale open folds characterize the more competent strata of the Mackenzie Platform to the east (Gordey and Anderson 1993).

Stratigraphy of the Howards Pass district

Carbonaceous and siliceous mudstones of the Ordovician to Silurian Duo Lake Formation (locally referred to informally as Howards Pass formation) of the Road River Group host most of the Zn-Pb deposits and occurrences (Fig. 3). The stratigraphy in the district is probably more complex than originally defined by Morganti (1979), owing to disruption of the succession by district-scale and local faults as revealed by recent geologic mapping (Hodder et al. 2014; Martel 2015). Specifically, previously reported thicknesses of stratigraphic units in some cases may represent structural repetitions (Hodder et al. 2014).

The basal sedimentary unit in the district (Fig. 3) is the Rabbitkettle Formation, consisting of massive and wavy banded limestone, silty limestone, and graded and laminated micrite beds, which together indicate an off-shelf, quiet-water, below wave-base depositional setting (Morganti 1979). The Transition zone that overlies the

Rabbitkettle Formation was interpreted in early studies as a separate unit, deposited in a similar stratigraphic setting as the Rabbitkettle Formation. However, due to a higher silica/carbonate ratio, Morganti (1979) suggested that the Transition zone was deposited in deeper parts of the basin, below the carbonate compensation depth. In contrast, Hodder et al. (2014) recently demonstrated that structures and textures within the wavy banded limestone represent highly strained to mylonitic features, with strain gradients increasing toward the upper contact with the Duo Lake Formation. Following this recent model, the Transition zone is considered a major detachment surface at the base of the Duo Lake Formation in the Howards Pass district, and therefore is not a separate stratigraphic unit.

The Duo Lake Formation consists of distinct member subdivisions that have been followed by all subsequent workers; from base to top these consist of: (1) Pyritic mudstone member; (2) Calcareous mudstone and overlying Cherty mudstone (combined as Cherty carbonaceous mudstone on Fig. 3); (3) Active mudstone; and (4) Upper siliceous mudstone (Fig. 3). The Pyritic member ranges from 2 to 10 m in thickness and is dark grey and typically finely laminated (Morganti 1979); pyrite and dolomite are volumetrically minor. This unit is overlain by massive to poorly bedded, dark grey calcareous mudstone at the base, transitioning to siliceous and carbonaceous mudstone at the top. Locally present are microscopic concretions of calcite-pyrite (Morganti 1979). The overlying Active mudstone member hosts nearly all of the Zn-Pb deposits in the district, and ranges in thickness from about 20 to 50 m. It consists of intercalated carbonaceous mudstone, cherty mudstone, and minor chert and limestone. Sulphide lenses within this unit consist of layered, laminated, and massive sphalerite ± galena,

189 variably deformed by shears and mylonite zones. Pyrite forms thin laminae of fine-
190 grained framboids; apatite is generally present in minor amounts. Overlying the Active
191 member is the Upper siliceous mudstone, which is commonly 20 to 90 m but locally up
192 to 120 m thick in the Howards Pass district and comprises dark grey to black mudstone
193 and minor chert (Morganti 1979) with locally abundant, thin (<1 cm) laminae of fine-
194 grained phosphorite (Goodfellow and Jonasson 1986; Slack et al. 2012). Orange-
195 weathering, silicic, bioturbated mudstone of the Silurian Steel Formation (Flaggy
196 Mudstone Formation in Howards Pass district) overlies the Duo Lake Formation and is
197 an important regional marker unit for stratigraphic correlation (Fig. 3).
198 Contacts between and within units from the upper Rabbitkettle Formation to the
199 lower Earn Group have been locally tectonized such that internal stratigraphy is disrupted
200 by complex thrust imbrication along detachment surfaces (Hodder et al. 2014; Martel
201 2015). As stated above, a prominent flat-lying décollement or zone of ductile and/or
202 brittle deformation occurs at the base of the Duo Lake Formation. Imbricate thrust faults
203 rise stratigraphically upward from this detachment surface and form the floor thrust of the
204 duplex structure that dominates the Howards Pass district (Fig. 3; Hodder et al. 2014).
205
206 Depositional environment of mudstone host rocks
207 Whole-rock analyses obtained from drill cores in relatively undeformed parts of
208 the deposits show that black mudstones of the Duo Lake Formation contain variable
209 silica (up to 90 wt % SiO_2) and carbonaceous or graphitic material (up to 16.5 wt % total
210 organic carbon, TOC; n = 58) (Slack et al. 2012). Ratios of redox-sensitive trace
211 elements, used to determine redox conditions in bottom waters, suggest that sulphidic or

anoxic conditions prevailed during deposition of the Cherty calcareous and Active mudstone members, leading up to and continuing during Zn-Pb mineralization (Slack et al. 2012), assuming that deposition of sulphide minerals was concurrent with sedimentation. Iron speciation data, sulphur isotope values of pyrite, and bulk Fe/Al and Mo/TOC ratios generally corroborate this redox interpretation (Johnson et al. 2014).

The age of the Duo Lake Formation was initially assigned on the basis of graptolite assemblages to straddle the Ordovician-Silurian boundary (Morganti 1979). Conodonts from the mineralized Active mudstone member further constrain the age to early to middle Llandovery as defined by Norford and Orchard (1985). Coeval Late Ordovician to early Silurian carbonate rocks east of Howards Pass in the Mackenzie Mountains record deposition in primarily shallow subtidal and evaporitic conditions (Pope and Leslie 2013).

Similar Paleozoic CD Zn-Pb deposits in the region

Other Paleozoic CD Zn-Pb deposits in the Selwyn Basin (Goodfellow 2004, 2007) are presumed to have formed at different times in the Paleozoic. The Dy, Vangorda, Faro, Grum, and Swim deposits in the Anvil district (Figs. 1 and 3) are hosted in lower Cambrian metasedimentary and minor metavolcanic rocks. Stratigraphically far above the Howards Pass deposits are the Tom and Jason deposits in the Macmillan Pass district (Fig. 1), hosted in Upper Devonian coarse clastic sedimentary rocks of the Earn Group. CD Zn-Pb deposits of the Gataga district, also known as the Kechika Trough of northern British Columbia, are hosted in Upper Devonian carbonaceous shale and chert of the lower Earn Group.

Howards Pass deposits

Active exploration for lead and zinc in the late 1960s and early 1970s led to the staking of the Howards Pass district in 1972. Throughout many years of exploration, at least 15 mineralized zones have been identified, including the XYC, Anniv, DON, and OP deposits that occur in a ~38-km-long, northwest-trending belt (Fig. 2). In 2010, China's Yunnan Chihong Zinc and Germanium Co. Ltd signed a joint venture agreement with Selwyn Resources Ltd., and in June, 2013, Selwyn Chihong Canada Mining Ltd. became the project's sole owner (Kirby 2014). Collectively, the Howards Pass deposits contain 185.6 Mt of drill-indicated resources at an average grade of 5.20% Zn and 1.79 % Pb, and 237.9 Mt of inferred resources at 4.47% Zn and 1.38% Pb; total resources are 423 Mt at 4.84% Zn and 1.59% Pb (Kirkham et al. 2012).

Stratigraphic sequences of the Duo Lake Formation are similar in all deposits. Each mineralized zone, averaging about 12 m in thickness, occurs at the same general stratigraphic position (Fig. 4), with high grade zones located preferentially at the base and top of the Active member (Kirkham et al. 2012). On this basis, it is assumed that all deposits formed concurrently. Available Pb isotopic data for sulphides and host rocks indicate that the major deposits (XYC, DON, OP, Anniv) formed from isotopically identical hydrothermal fluids, thus supporting a cogenetic model (Cousens 2007), although multiple mineralizing events in the district cannot be ruled out.

The Zn-Pb deposits are situated along the limbs of major synclinal structures that formed during Mesozoic deformation. This deformation also resulted in imbricate thrust faults and the development of several cleavage sets (McClay 1991; Hodder et al. 2014).

Low grade, subgreenschist-facies metamorphism affected rocks in the Selwyn Basin at ~125-120 Ma (Gabrielse and Yorath 1989), but no metamorphic grade indicator minerals have been identified within the shales or mudstones (McClay 1991). Rather, the key evidence for regional temperature levels derives from reflectance values of graptolites (Riediger et al. 1989), and Conodont Alteration Indices (CAI) that reflect thermal maturity of conodonts and by inference host strata (Epstein et al. 1977). In pre-Cretaceous rocks of the Selwyn Basin, CAI values are 4-5 (Gordey and Anderson 1983; MacNaughton et al. 2008), indicating temperatures of ca. 300° to 400°C during deformation and burial metamorphism. However, despite unquestionable overprinting of textures by low-grade metamorphism and penetrative deformation, many primary depositional and diagenetic features are still preserved within the Howards Pass Zn-Pb sulphides and host strata (Jonasson and Goodfellow 1986; Gadd et al. 2016).

Mineralogical and textural characteristics of ore

Texturally and mineralogically, all of the Zn-Pb deposits are similar (Morganti 1979; Goodfellow 2004). The Anniv, XYC, and DON deposits are the most economically significant within the belt (Mining Yukon 2014). Types of mineral textures include (1) relatively undeformed interlaminations of sulphides and carbonaceous mudstones, having typical grain sizes of less than 250 μm (Fig. 5b and d); (2) microfolds composed of fine and coarse sulphide laminations and layers (Fig. 5a, c, and f); and (3) sulphide-bearing cleavages, veinlets, and thin fractures that cut bedding and sulphide laminations (Fig. 5g and h). Given that the objective of this study is to determine the age of the laminated sulphides, only the first two of these textural types are discussed. Diverse tectonic

281 structures that are superimposed on the layered rocks are described in detail by Jonasson
282 and Goodfellow (1986) and McClay (1991).
283
284 *Laminated sulphide zones*
285 Individual layers within the laminated sulphide zones range from <0.05 mm to as
286 much as 1 cm thick (Fig. 5a). The fine-scale laminations are represented largely by color
287 variations caused by different proportions of organic matter and quartz intermixed with
288 sulphides (Fig. 6g). Principal minerals in the laminated ore are sphalerite, galena, and
289 pyrite. Chalcopyrite and molybdenite are reported (Goodfellow 2004), but were not
290 observed in samples examined for this study. Barite is absent, although it occurs in
291 overlying Devonian carbonaceous chert and mudstone in the Howards Pass district and
292 regionally (Morganti 1979; Goodfellow 2004, 2007).
293 Pyrite is mainly framboidal to cubic (Fig. 6), comprising irregular masses
294 intergrown with mudstone and other sulphide minerals (Jonasson and Goodfellow 1986;
295 Gadd et al. 2016). The framboids typically range in size from <5 to at least 50 μm (Fig.
296 6a, b, e, h), but are locally as large as 200 μm. Thin beds composed of graded framboids
297 occur locally (Jonasson and Goodfellow 1986). Some framboids display well-preserved
298 internal structures, whereas others lack internal features (Fig. 6h). Although discrete
299 framboids are present, pyrite framboids typically coalesce and form irregular masses.
300 Bedding-parallel layers of pyrite are evident in some samples (Fig. 6d, g). Pyrite also
301 forms euhedral cubes 0.1 to 0.4 mm in diameter (Fig. 6c); locally, euhedral pyrite occurs
302 as overgrowths on earlier framboidal pyrite and sphalerite (Fig. 6c, h) or is overgrown by
303 sphalerite (Fig. 6a).

Sphalerite grains are concentrated in zones within pyrite-rich layers (Fig. 6d, e), typically in a quartz- or mudstone-rich matrix among pyrite framboids (Fig. 6h, i). The edges of some framboids in the sphalerite-filled matrix are commonly obscured (Fig. 6h, i). Sphalerite also forms inclusions within euhedral pyrite (Fig. 6c), and elongate grains parallel to bedding (Fig. 6g). Individual sphalerite grains are about 5 to 60 μm in diameter. Where present, galena is most common as inclusions in sphalerite, although Gadd et al. (2016) report interlaminations of sphalerite with galena and framboidal pyrite.

Mudstone host rocks are locally fossiliferous and in places the sulphide minerals partially replace fossils. An abundance of undeformed microfossils in calcareous lenses and concretions within the Active mudstone include various forms of algae, mazuelloids, and other organic debris (Jonasson and Goodfellow 1986). One sample of unmineralized mudstone from drill core (XYC116-365.8 m), about 4.6 m below the Active member, contains abundant (~20 vol % of the rock) well-preserved radiolarians and sponge spicules (J.A. Dumoulin, U.S. Geological Survey, written communication, 2014). Most of the radiolarians in this sample are ~100-200 μm in diameter, and are similar in appearance to those in calcareous radiolarite layers contained within mudstone in the Red Dog deposit area (Dumoulin et al. 2004). Sponge spicules in unmineralized mudstone from Howards Pass include simple forms with hollow centers (20-40 x 100-950 μm), typically filled with polycrystalline silica or organic matter (J.A. Dumoulin, U.S. Geological Survey, written communication, 2014). Circular features in sulphide samples could either be pyritized radiolarians (Fig. 6j) or cross sections of sponge spicules (Fig. 6a, i), suggesting that in some cases pyrite preferentially replaced the rims and/or central cores of spicules; silica or organic matter typically makes up the core, but sphalerite has

clearly replaced spicule cores in places. Alternatively, these small rounded features may be pyrite framboids with centers composed of algal and mazuelloid fossils, which are locally replaced by sphalerite (Jonasson and Goodfellow 1986).

Microfolds

Folding of sulphide layers is interpreted to have occurred both during compaction of the sediments and post-sedimentation tectonic deformation. Folded and contorted layers that resulted from compaction (Fig. 5a, c, f) are locally overprinted by recrystallization and the development of pressure-solution cleavages and sulphide-bearing shears and mylonitic features (Fig. 5e, g, h) (McClay 1991). In many folded layers, individual laminae remain predominantly parallel (Fig. 5f) accompanied by some thinning or pinching (Fig. 5c). Within relatively thicker pyritic layers (Fig. 5a), ptygmatic-like folds are present, interpreted as having formed during compaction and final dewatering (Jonasson and Goodfellow 1986). Fold hinges may contain as much as 50 vol % sphalerite with grains up to 100 μm across, a product likely resulting from structural thickening of sphalerite-rich laminae. High-grade galena mineralization preferentially occurs as cleavage-controlled stringers (Gadd et al. 2016) and with sphalerite in the hinge zones of folds (Morganti 1979).

Methods

Twelve samples of sulphide-rich rock collected from exploration piles and drill cores at the XYC and DON deposits were examined petrographically. Three samples from XYC and one from DON containing layered and laminated sulphides were selected for further study and processing for Re-Os analysis (Table 1; Fig. 5a, c, e, and f). Two of

351 the three XYC sulphide-bearing samples were divided into two or more subsamples in
352 order to obtain multiple pyrite separates from each sample. Additionally, two samples
353 from the XYC deposit (XYC-txt3 and XYC-txt4) were sieved to yield fine (<0.25 mm)
354 and coarse (~0.25 to 0.5 mm) pyrite separates (indicated by "f" or "c" suffix,
355 respectively; Table 1). Sample XYC-127-124.5 lacked sufficient pyrite for multiple
356 separates and therefore a single bulk separate was obtained.
357 The DON mineralized sample was collected from drill core (DON-137-303.8).
358 This sample yielded only a fine-grained fraction of pyrite; consequently, the rock was cut
359 into four sections and pyrite separates were obtained for each.
360 One unmineralized carbonaceous mudstone ~19.6 m stratigraphically below the
361 Zn-Pb-bearing zone (Active mudstone) was collected from drill core at the DON deposit
362 (DON-111-157.8; Table 1). This bulk sample was subsequently processed and ground to
363 a powder.
364 A total of 12 pyrite mineral separates of ~200-400 mg was obtained using
365 traditional isolation methods (crushing, magnetic and/or heavy liquid separation,
366 handpicking). Care was taken to isolate pyrite from the matrix of the mudstone and to
367 ensure that pyrite was free of mudstone fragments adhered to grain surfaces. However,
368 mudstone inclusions within pyrite cannot be visually identified during handpicking.
369 Evidence for the presence of mudstone inclusions was recorded by a white grainy residue
370 that remained after digestion of the separate in inverse *aqua regia* (Table 1), as described
371 below.
372 The Re-Os analyses were conducted at the Source Rock and Sulfide
373 Geochronology and Geochemistry Laboratory at Durham University, Durham, U.K.

Pyrite separates were weighed and loaded into a Carius tube with a known quantity of mixed Re-Os tracer solution containing ^{185}Re and ^{190}Os. Using the Carius tube method, sample and tracer solution were digested and equilibrated using a mixture of 11N HCl (3 ml) and 15.5N HNO_3 (8 ml) (inverse *aqua regia*) at 220°C for 48 hours (Selby et al. 2009). A weighed aliquot of the unmineralized mudstone sample was also digested in a Carius tube containing mixed ^{185}Re and ^{190}Os tracer solution with 8 ml of 4N H_2SO_4 bearing 0.25g/g CrO_3 for 48 hours at 220°C (Selby and Creaser 2003).

The acidic medium, *aqua regia*, digests sulphide minerals and organic matter. The latter is a significant component of unmineralized mudstones in the Howards Pass district. For example, the 10-m-thick mudstone interval from which the unmineralized bulk sample was collected contains 8.6 to 16.0 wt. % TOC (n = 4). Organic matter-bearing sedimentary rocks, such as mudstones, are commonly enriched in Re and Os (Selby and Creaser 2003; Selby et al. 2009). Silicate minerals such as quartz, muscovite, and clays present in mudstone of this study are coated with organic matter. These silicate minerals are resistant to digestion in *aqua regia*. Six of the pyrite separates used in this study contained a silicate residue after dissolution (Table 1). The presence of a silicate residue signifies the strong likelihood that submicroscopic amounts of organic matter from the mudstone had been present (but dissolved with pyrite) in the separate as fine intergrowths with, or contained within, pyrite, or as coatings on grains. Hence, the resulting Re-Os data obtained likely represent a mixture of Re and Os liberated from both pyrite and organic matter. Conversely, the lack of any detectable residue after digestion supports the high purity of these mineral separates, and the absence of any Re and Os incorporated from organic matter.

Following Carius tube digestion, osmium was isolated and purified from the acidic digestion medium using solvent extraction ($CHCl_3$) and micro-distillation methods (Selby and Creaser 2001). Rhenium was then isolated from the resulting Os-extracted acid medium by anion-column and single-bead chromatography methods (Selby and Creaser 2003). The purified Re and Os were loaded onto Ni and Pt filaments, respectively (Selby et al. 2007). Isotopic measurements were conducted using negative thermal ionization mass spectrometry (Creaser et al. 1991) on a Thermo Scientific TRITON mass spectrometer via ion-counting, using a secondary electron multiplier in peak-hopping mode for Os, and static Faraday collection for Re. Total procedural blanks during the course of this study for Re and Os were 3.5 ± 0.4 and 0.7 ± 0.8 pg, respectively, with an average $^{187}Os/^{188}Os$ value of 0.25 ± 0.05 (1SD, n = 3). All uncertainties are determined by error propagation of uncertainties in Re and Os mass spectrometer measurements, blank abundances and isotopic compositions, spike calibrations, and the reproducibility of standard Re and Os isotopic values. In-house solution standards run during the course of the study (in 2010) are 0.16084 ± 0.00013 (1SD, n = 3) for DROsS and 0.5984 ± 0.0012 (1SD, n = 3) for Re Standard solution, which are in agreement with those reported previously (Nowell et al. 2008; Cumming et al. 2012, and references therein).

Regression of the Re-Os data and independent calculation of initial $^{187}Os/^{188}Os$ ratios (Os_i) is carried out using *Isoplot V. 4.15* (Ludwig 2003) and the ^{187}Re decay constant of 1.666×10^{-11} a^{-1} (Smoliar et al. 1996), respectively.

Re-Os results

Re-Os analyses were obtained for all 12 pyrite separates and one unmineralized organic-rich mudstone (Table 1). Based on geological and stratigraphic similarities (Fig. 4) and textural observations (Figs. 5 and 6) between the Zn-Pb deposits, sulphide mineralization at XYC and DON is considered to be penecontemporaneous. However, given the spatial separation of these two deposits (ca. 12 km), and significant differences in Re and Os abundances of the pyrite separates, Re-Os data for the XYC and DON samples are initially considered separately (Fig. 7).

Rhenium and Os concentrations in the eight XYC separates range from 2.2 to 21.4 ppb, and 93.4 to 692.3 ppt, respectively (Table 1). The $^{187}Re/^{188}Os$ data show a limited range of values (137.6 to 209.7), but the measured $^{187}Os/^{188}Os$ ratios display more variability (1.723 to 3.128). The Re-Os data as a whole lack a statistical meaningful isochron age (156 ± 1200 Ma; MSWD = 543; Fig. 7A). Based on the biostratigraphic age of the host rock (Active member, ~442 Ma), Os_i values range from 0.47 to 2.04. Among these eight separates, only three have similar values (Os_i = ~0.7; Table 1). These three are the only XYC separates that did not yield a residue after acid digestion. Hence, they are considered to record the Re-Os systematics solely of pyrite and not a mixture derived from pyrite and organic matter contained in mudstone, potentially present as coatings and/or microscopic inclusions in the pyrite. Data for the other separates are interpreted to represent a mixture of Re and Os derived from pyrite and organic matter based on the presence of a silicate residue following digestion. The three separates with similar Os_i values (~0.7) also possess similar Re-Os isotope values, and as a result, the regression of the Re-Os data yields an imprecise isochron age of 480 ± 570 Ma (MSWD = 6.8; Fig. 7a).

Only one of four pyrite separates from the DON deposit sample yielded a silicate residue after digestion (Table 1). Collectively, the four separates have Re and Os abundances of 33.6 to 37.0 ppb and 599.8 to 694.9 ppt, respectively. With the exception of the Re-Os data for DON-137(1), the Re-Os isotope compositions are similar, and do not yield a geologically meaningful isochron age (2075 ± 1700 Ma; MSWD = 85; Fig. 7B). Furthermore, the DON separates (excluding DON-137(1)) yield Os_i values similar to those of three of the XYC separates (~0.7; Table 1). The DON separates possessing similar Os_i values have very similar Re-Os isotope values, which yield a highly imprecise isochron age of 457 ± 1500 Ma (MSWD = 19; Fig. 7B). Nominally, this age is very similar to that obtained for the XYC separates.

As stated above, separates that did not yield a significant silicate residue following acid digestion provide the best record of the Re-Os isotope systematics of pyrite, and contain limited to no evidence of Re and Os derived from organic matter that occurred as coatings on grains or intergrowths with pyrite. Data for these six separates produce a Re-Os isochron age of 442 ± 14 Ma (MSWD =7.4) and an Os_i value of 0.71 ± 0.07 (Fig. 8).

The unmineralized black calcareous and carbonaceous mudstone sample (DON-111-157.8) that was collected ca. 20 m below the Active member in the footwall of the Zn-Pb mineralized zone consists of organic matter, calcite, quartz, muscovite, pyrite, and dolomite (Morganti 1979). The sample contains 51 ppb Re and 1.6 ppb Os (1632 ppt Os), and $^{187}Re/^{188}Os$ and $^{187}Os/^{188}Os$ values of ~197 and 2.505, respectively (Table 1). The Re-Os data yield an Os_i value (calculated at 442 Ma) of 1.05 ± 0.01. Because the sampled interval is ca. 20 m below the mineralized Active member, it was likely deposited

thousands or millions of years earlier. However, even a few million years will not appreciably affect the calculated Os_i value. For example, at 445 Ma, the calculated Os_i is 1.04.

Discussion

Temporal relationships between pyrite and sphalerite

The laminated nature of the Zn-Pb sulphide zones in the Howards Pass district has been attributed to predominantly exhalative processes of mineralization (Jonasson and Goodfellow 1986; Goodfellow 2007). In contrast, a Middle Jurassic paleomagnetic age was obtained on coarse-grained sulphide-rich rock (Kawasaki and Symons (2012). These authors suggest that the laminated sulphides also possibly, but less likely, formed during the Mesozoic. The aim of the present study is to use the Re-Os chronometer on pyrite from Howards Pass to determine an absolute age of Zn-Pb mineralization for the layered and laminated sulphides. In order to do so, documentation of a linked paragenesis of pyrite and sphalerite is necessary. Such documentation is not straightforward, because the Howards Pass deposits have been affected by post-ore deformation and metamorphism.

Pyrite in the Howards Pass laminated sulphide zones occurs as framboids <5 to 200 μm in diameter, euhedral overgrowths on framboids, and as concentrations of subhedral and euhedral grains within relatively thick layers (Figs. 5 and 6). Abundant framboidal pyrite is typical of some other CD Zn-Pb deposits such as Citronen Fjord in North Greenland (Kragh et al. 1997) and HYC in northern Australia (Williams 1978). On the other hand, many large CD Zn-Pb ores lack abundant framboidal pyrite (e.g., Red Dog; Kelley et al. 2004b). The presence of framboidal pyrite does not necessarily

indicate formation during sedimentation because it may form tens to hundreds of millions of years after deposition of the host rocks, during late diagenesis, low-grade metamorphism, and/or hydrothermal alteration (Scott et al. 2009). However, based on analogy with modern marine environments (Canfield et al. 1992; Wilkin and Barnes 1997; Wilkin et al. 1997) and textural studies of other unmetamorphosed CD Zn-Pb deposits (e.g., Williams 1978; Kragh et al. 1997), framboidal pyrite in the Howards Pass sulphide deposits most likely formed in anoxic or sulphidic pore fluids within centimeters of the sediment-water interface, or in some cases in sulphidic bottom waters. The overgrowths of euhedral pyrite on framboidal pyrite also probably formed early, during diagenesis as suggested by similarities in trace and minor element contents and spatial associations between this type of pyrite and the framboidal pyrite (Gadd et al. 2016).

Sphalerite in the laminated sulphide zones typically forms the matrix between framboidal pyrite grains (Fig. 6a, c, f), and although not observed in this study, some framboidal pyrite grains have reported cores of sphalerite (Goodfellow and Jonasson 1986), suggesting that in places sphalerite predated or was concurrent with early pyrite formation. In some laminae, sphalerite is intergrown with or encased by euhedral pyrite (Fig. 6b, d, h). If the euhedral pyrite formed during sedimentation and diagenesis as suggested by Gadd et al. (2016), then by inference the sphalerite inclusions within euhedral pyrite also formed at this time, or earlier. Some sphalerite and pyrite show evidence of selective replacement of fossils (Fig. 6a, h, i), which argues for subseafloor precipitation of these sulphides. However, such textures do not conclusively determine the timing between pyrite and sphalerite deposition. Although numerous examples exist of intergrowths between sphalerite and pyrite (Fig. 6b, h), observed textures do not

preclude the formation of sphalerite after framboidal pyrite. Primary textural features assumed to represent synsedimentary exhalative (SEDEX) co-precipitation of sulphide minerals may also result from the subseafloor replacement by sulphide of carbonate layers within mudstone during sedimentation and early diagenesis (e.g., Anarraaq deposit, northern Alaska; Kelley et al. 2004a), or by replacement many millions of years after sedimentation (Leach et al. 2005). Therefore, carbonate cement in the Howards Pass mudstones, preserved long after pyrite formation, could have been later replaced by sphalerite. However, without compelling textural evidence to support such a late paragenesis for sphalerite (e.g., overgrowths on euhedral pyrite or crosscutting relationships), the simplest model is one in which pyrite and sphalerite within the laminated sulphides formed concurrently, during sedimentation and/or diagenesis.

Purity of pyrite separates

Based on the fine-grained nature (typically <250 μm) and intergrowths of pyrite and sphalerite at Howards Pass, much of the pyrite likely contains sphalerite fragments or inclusions (e.g., Fig. 6b; Gadd et al. 2016). However, because sphalerite typically contains less Re and Os (e.g., orders of magnitude lower concentrations in sphalerite compared to pyrite in massive ore from Red Dog; Morelli et al. 2004), the Re-Os systematics of pyrite are likely unaffected by sphalerite inclusions.

The finely intergrown nature of pyrite and mudstone in our samples presented the greatest challenge to obtaining pure pyrite separates. Impure separates can yield Re-Os data that do not record the age of the pyrite, but rather a mixed age that reflects Re-Os systematics of both the pyrite and the organic component of mudstone, the latter

potentially having high Re and Os contents (Selby and Creaser 2003; Selby et al. 2009). Therefore, it is critical to document the purity of the pyrite separates in order to provide a robust interpretation of the age data.

Most pyrite separates were hand-picked after heavy liquid and magnetic separations. Pyrite grains having visible mudstone intergrowths were excluded, but mudstone inclusions within pyrite or coatings of organic matter on grains cannot be identified visually during hand picking. Six of the 12 pyrite separates contained residual minerals (quartz, muscovite, clays hosted in mudstone) following digestion with *aqua regia* at 220°C (Table 1). Given that organic matter coats grains and/or occurs as submicron inclusions in pyrite, occurrence of the residue signifies that organic matter was likely present and dissolved with the pyrite. As a result, the Re and Os budget will include both that of dissolved pyrite and organic matter. The six separates that produced a silicate residue have widely varying calculated Os_i values (-0.77 to 2.04) that are distinct from the ~0.7 value of other pyrite separates that are considered to be pure and lack mudstone inclusions or coatings. The wide variation in the Os_i values is consistent with studies that have shown heterogeneity of Re and Os contents in organic matter, especially in <10 g samples. In cases where Re and Os covary inconsistently, the resulting Os_i value will be highly variable (Kendall et al. 2009).

Based on the above discussion, only pyrite separates that did not yield silicate residues after digestion are considered to record the Re-Os systematics solely of pyrite and not a mixture between those of pyrite and organic matter contained in mudstone. The purity with respect to mudstone or organic matter inclusions within these pyrite separates is assumed to be 90% or greater (referred to as pure pyrite).

The Re and Os concentrations of pure pyrite separates from the DON deposit (34.0–37.0 ppb and 636.8–694.9 ppm, respectively; Figs. 4f and 5g-i) are distinct compared with those of pure pyrite from the XYC deposit (2.2-4.0 ppb and 93.4 to 123.4 ppb; Figs. 4a, e and 5). Even if small amounts of mudstone still remained in the separates, a comparison of pyrite compositions suggests that this is not the cause of the large differences in Re contents (~30 ppb) between the DON and XYC separates. The Re content of unmineralized mudstone from the DON deposit is only 50.85 ppb (Table 1), and therefore an unrealistically large component of mudstone would be necessary to increase Re contents of the pyrite sample by 30 ppb. Hence, contamination by mudstone is considered quantitatively unimportant and thus unlikely to account for the differences in pyrite Re and Os isotope values determined for the XYC and DON deposits.

Because the objective of this study is to determine the age of the early stage of mineralization that produced the laminated sulphides and not the later coarse-grained veins, the separates also require purity with respect to pyrite type or stage. Most hand samples chosen for processing are finely laminated and free of any apparent coarse-grained veins (Fig. 5). However, one hand sample (XYC-txt3) has obvious later veining (Fig. 5e) and although the late veins were avoided during processing, it is possible that late coarse pyrite was incorporated in the mineral separates. Fine-grained (<0.25 mm) and coarse-grained (~0.25 to 0.5 mm) fractions of pyrite from this sample lack significant variation in Re and Os concentrations or isotope ratios (Table 1). Interestingly, most separates that were excluded based on the presence of residues are fractions from the XYC-txt3 sample, and two of these are coarse-grained (Table 1). If late pyrite is present in these separates, it may explain why the Re-Os data from all XYC separates lack a

580 statistically meaningful isochron age (Fig. 7a). Regardless, these samples were not used
581 in the final age calculation.
582
583 Age of host rocks and mineralized zones
584 Biostratigraphic data for the Howards Pass region include graptolite and conodont
585 ages (Fig. 9). Notably, many uncertainties in the biostratigraphic ages arise from poor
586 preservation and/or undiagnostic character (Norford and Orchard 1985). Graptolites are
587 rare and poorly preserved, and within the Howards Pass district all known occurrences in
588 the Active mudstone are sheared (Norford and Orchard 1985). However, units
589 stratigraphically above and below contain graptolites in zones at least 0.2 m thick.
590 Graptolites at the top of the Upper siliceous mudstone member and in the footwall
591 Calcareous mudstone unit bracket the mineralization age to Late Ordovician or early
592 Silurian (Morganti 1979). Two samples of black mudstone from a stratigraphic section
593 about 20 km southwest of Howards Pass yielded graptolites of early Llandovery and
594 middle Llandovery age as interpreted by Norford and Orchard (1985), but this mudstone
595 is not mineralized and therefore its direct correlation with the Active member is
596 conjectural (Fig. 9).
597 Seven conodont samples collected from the Duo Lake Formation northwest of the
598 Howards Pass district were determined to be of Late Ordovician to early Silurian age
599 (McCracken 2014). Within the district, biostratigraphic ages for the Active mudstone
600 member and overlying units are based on conodonts that were obtained not only from
601 outcrop but also drill cores (Norford and Orchard 1985). Pyritized fragments of
602 radiolarians recovered from the Active mudstone are not diagnostic (F. Cordey,

University of Lyon, written communication, 2014), but conodonts from the ore zone are diagnostic, although relatively small (<1.5 mm). Most conodont species in the Active member were reported by Norford and Orchard (1985) to represent the *kentuckyensis* zone; these resemble representative species that may have coexisted in the *Distomodus kentuckyensis* zone (Norford and Orchard 1985), which equates to absolute ages ranging from ~443.8 to 441 Ma (Fig. 9) based on the geologic time scale of Gradstein et al. (2012).

Ambiguities and uncertainties in biostratigraphic ages and correlation with regional units in the district illustrate the need to directly date mineralizing events. Assuming that Fe and Zn-Pb sulphide minerals formed contemporaneously, the Re-Os age of pyrite may be used to indirectly date the base-metal event. Textures of sulphide samples from the Howards Pass deposits are suggestive of coeval deposition of pyrite and sphalerite. If this assumption is incorrect, an age determination for pyrite at least provides a maximum age of sphalerite mineralization.

An important observation regarding the Re-Os systematics in pyrite from the Howards Pass district is that although samples from different deposits (DON and XYC) have highly variable Re and Os abundances, as well as $^{187}Re/^{188}Os$ and $^{187}Os/^{188}Os$ ratios (Table 1), the data collectively yield a well-defined regression with a Re-Os isochron age of 442 ± 14 Ma (Fig. 8). This age is consistent with the early Llandovery biostratigraphic age of the host rocks (Fig. 9), and suggests that mineralization occurred during the early Silurian, concurrent with sedimentation or early diagenesis. Formation of the stratiform Zn-Pb deposits during the Jurassic-Cretaceous (Kawasaki and Symons 2012) is ruled out

by this isochron age, excluding the remobilization of coarse sulphides into late fractures that likely occurred in the Mesozoic.

Re-Os isotope compositions and source implications

The 15 sites of known Zn-Pb mineralization that occur ca. 38 km along strike in the Howards Pass district (Fig. 2) are similar with respect to stratigraphic, textural, geochemical, and mineralogical characteristics (Figs. 4-6). These similarities suggest that the individual deposits and occurrences are part of the same hydrothermal system, supported by Pb isotope data for sphalerite and galena from several of the deposits that indicate mineralization formed from isotopically homogeneous fluids (Cousins 2007). Although it has been proposed that the northwest-trending belt of deposits resulted from deposition in separate local sub-basins (Morganti 1979; Goodfellow 2004, 2007), the recent work of Hodder et al. (2014) suggests that the northwest trend instead is a structural artifact of the surface traces of parallel, southwest-dipping thrust faults.

If the assumption is correct that mudstone inclusions in pyrite are not the cause of the variability in Re and Os abundances, and that the deposits formed from the same or similar hydrothermal fluids, alternative explanations are needed for the observed differences in Re and Os systematics between the XYC and DON deposits. Notably, it is not uncommon for pyrite within a single sulphide deposit to possess highly variable Re and Os abundances. For example, the Re and Os abundances of pyrite separates from massive sulphide ores at Red Dog (~351–383 ppb Re, 3353–3637 ppt Os) are greatly different from those of pyrite in vein ore (~14–31 ppb Re, 98–235 ppt Os) from a different part of the deposit (Morelli et al. 2004), and those of pyrite from silicified wall

rocks at Red Dog (~2.7–34 ppb Re, 85–789 ppb Os; Slack et al. 2015). Furthermore, pyrite and other associated sulphides composing modern deep-sea massive sulfide deposits show highly variable Re and Os abundances (0.1–74 ppb Re, 2–54 ppt Os; Zeng et al. 2014). The variations in Re and Os isotopic composition of pyrite from the DON deposit compared with those from the XYC deposit may reflect differences in Re and Os concentrations in the mineralizing fluids. Such differences may be due to changing fluid chemistry or redox conditions (e.g., Re is highly mobile under oxidized conditions and precipitates under reduced conditions) with time, deposition in different portions of the deposit, or derivation of Re and Os from different sources as observed for massive sulfide deposits in modern seafloor-hydrothermal systems (Zeng et al. 2014).

The Os_i values of sulphides and host rock provide additional information about the sources of metals. The Os_i value calculated from the pyrite Re-Os isochron is 0.71 ± 0.07 (Fig. 8). The single sample of unmineralized mudstone collected ~20 m stratigraphically below the Active mudstone has an Os_i value of 1.05 (calculated at 442 Ma; Table 1), which is nearly identical to that of modern seawater (e.g., Peucker-Ehrenbrink and Ravizza 2000). It could be argued that this sample may not record the Os_i of coeval seawater during sulphide deposition, for two reasons: (1) because the sampled interval is 20 m below the mineralized Active mudstone, and could represent thousands or millions of years of intervening sedimentation, and (2) because the residence time of Os in seawater is short (~10 to 20 ka; Steele et al. 2009). However, even if we consider the unmineralized mudstone to be 3 m.y. older than the active mudstone unit (Late Ordovician, Late Hirnantian), the calculated Os_i value does not appreciably change (Os_i at 445 Ma = 1.04). Of interest is that the Os_i value of 1.04 to 1.05 for mudstone in the

671 footwall to mineralization coincides with the highly radiogenic Os_i signature recorded
672 from the Global Stratotype Section and Point (GSSP) at Dobs Linn, Scotland, during the
673 deglacial phase of the Late Ordovician Hirnantian glaciation (Finlay et al., 2010).
674 The Os_i value of ~0.71 determined from the pyrite Re-Os isochron is similar to
675 that of earliest Silurian seawater recorded in mudstone from the basal Silurian section at
676 Dobs Linn after rapid deglaciation (Finlay et al. 2010). The nominal temporal agreement
677 of the pyrite Os_i value with the Dobs Linn mudrock value suggests a hydrogenous
678 (seawater) source for the Os. Based on the ~442 Ma age that indicates synsedimentary to
679 diagenetic sulphide precipitation at Howards Pass, two sources of Os are possible: (1) the
680 Zn- and Pb-bearing hydrothermal fluid, which leached Os from footwall sedimentary
681 rocks that were deposited in seawater; or (2) directly from seawater during precipitation
682 of the pyrite, which suggests that the Os content of the hydrothermal fluid was minor
683 relative to that of seawater. The latter scenario is consistent with recent studies that show
684 a predominant seawater-derived source of Os in modern seafloor massive sulphide
685 deposits (Zeng et al. 2014).
686 Based on regional geologic constraints and the textural, isotopic, and
687 geochronological data obtained from this study, a genetic model is proposed for the
688 Howards Pass deposits that is consistent with that proposed for CD Zn-Pb deposits
689 worldwide (Leach et al. 2005; 2010): (1) ore fluids originated as evolved, oxidized,
690 brines in shallow evaporative basins; silicified evaporate casts and the abundance and
691 diversity of macrofauna in shallow platform carbonate rocks in the Mackenzie Mountains
692 east of Howards Pass are evidence that warm-water, arid conditions prevailed in Late
693 Ordovician and early Silurian time (Pope and Leslie 2013); (2) the brines infiltrated and

694 circulated through underlying oxidized clastic rocks or fractured basement to depths of 3
695 to 5 km; (3) Pb and Zn were extracted and the metalliferous brines ascended into organic-
696 rich rocks that facilitated reduction of seawater or porewater sulphate to H_2S; and (4)
697 pyrite, sphalerite, and galena were deposited at or near the seafloor during sedimentation
698 and early diagenesis. The Zn- and Pb-bearing hydrothermal fluid may have leached Os
699 from seawater-deposited footwall sedimentary rocks, or Os was sourced directly from
700 seawater and incorporated in pyrite.
701

702 **Conclusions**

703 Pure (<10 vol % mudstone inclusions) pyrite separates obtained from laminated
704 sulphide zones in two different deposits (XYC and DON) have highly variable Re and Os
705 abundances, as well as $^{187}Re/^{188}Os$ and $^{187}Os/^{188}Os$ ratios, and collectively yield a well-
706 defined regression with a Re-Os isochron age of 442 ± 14 Ma. Similarity in stratigraphic,
707 textural, geochemical, and mineralogical characteristics among deposits in the district,
708 and previous Pb isotope compositions for galena and sphalerite from different deposits,
709 together argue for a single hydrothermal system, although individual mineralized centers
710 may represent deposition in separate local sub-basins. Observed variations in Re and Os
711 isotopic composition of pyrite between the two studied deposits may reflect differences in
712 Re and Os concentrations in the ore-forming fluids, perhaps due to changing fluid
713 chemistry (e.g., redox conditions) with time or space, including differences in relative
714 timing of sulphide deposition and/or depositional sites within the basin.
715 The initial Os isotope composition of mudstone in the footwall to mineralization
716 coincides with the highly radiogenic Os_i signature recorded from Dobs Linn during the

717 deglacial phase of the Late Ordovician Hirnantian glaciation and pyrite from mineralized
718 rocks at Howards Pass is similar to that of earliest Silurian seawater following rapid
719 deglaciation (Finlay et al. 2010), suggesting that (1) the Zn- and Pb-bearing hydrothermal
720 fluid leached Os from footwall sedimentary rocks that were deposited in seawater; or (2)
721 Os was derived directly from seawater during precipitation of the pyrite, which suggests
722 that the Os content of the hydrothermal fluid was minor relative to that of seawater.
723

724 **Acknowledgements**

725 We thank Jason Dunning and David Legault (formerly with Selwyn Resources
726 Ltd.) and Gabriel Xue (Selwyn Chihong Mining Ltd) for providing access to drill cores
727 and exploration reports, and logistical aid during field work. Edith Martel and Beth
728 Fisher (NTGO) and Bob Hodder (consultant) made our stay at camp possible and guided
729 us in learning the regional geology, sedimentology, and structure of the district. Matt
730 Jodrey (formerly Selwyn Resources Ltd) assisted with sampling of drill core and rock
731 slabbing. Julie Dumoulin (USGS) examined thin sections, provided petrographic
732 descriptions, and reviewed sections in this report on stratigraphy and biostratigraphic
733 ages. Reviews by Garth Graham, Marc Norman, Kat Suzuki, and AE David Huston
734 greatly improved the manuscript. DS acknowledges the support of the TOTAL
735 endowment fund. Any use of trade, product, or firm names is for descriptive purposes
736 only and does not imply endorsement by the U.S. Government.

737 **References**

738 Canfield DE, Raiswell R, Bottrell S (1992) The reactivity of sedimentary iron minerals
739 towards sulfide. Amer Jour Sci 292:659–683
740

741 Cousens BL (2007) Radiogenic isotope studies of Zn-Pb mineralization in the Howards
742 Pass area, Selwyn Basin. In: Falck H, Wright DF (eds) Mineral and energy resource
743 potential of the proposed expansion to the Nahanni National Park Reserve, north
744 Cordillera, Northwest Territories. Geol Survey Canada Open File 5344: 279–292
745
746 Creaser RA, Papanastassiou DA, Wasserburg GJ (1991) Negative thermal ion mass
747 spectrometry of osmium, rhenium and iridium. Geochim Cosmochim Acta 55:397–
748 401
749
750 Cumming VM, Selby D, Lillis PG (2012) Re-Os geochronology of the lacustrine Green
751 River Formation: insights into direct depositional dating of lacustrine successions,
752 Re-Os systematics and paleocontinental weathering. Earth Planet Sci Lett 359-
753 360:194–205
754
755 Dumoulin JA, Harris AG, Blome CD, Young LE (2004) Depositional settings,
756 correlation, and age of Carboniferous rocks in the western Brooks Range, Alaska:
757 Econ Geol 99:1355–1384
758
759 Dusel-Bacon C, Lanphere MA, Sharp WD, Layer PW, Hansen VL (2002) Mesozoic
760 thermal history and timing of structural events for the Yukon-Tanana upland, east-
761 central Alaska: 40Ar/30Ar data from metamorphic and plutonic rocks. Can Jour
762 Earth Sci 39:1013–1051
763
764 Eisbacher GH (1985) Late Proterozoic rifting, glacial sedimentation, and sedimentary
765 cycles in the light of Windermere deposition, western Canada. Palaeogeogr,
766 Palaeoclimatol, Palaeoecol 51:231–254
767
768 Epstein AG, Epstein JB, Harris LD (1977) Conodont color alteration—an index to
769 organic metamorphism. US Geol Survey Prof Paper 995, 27 pp
770
771 Feng C-Y, Qu W-J, Zhang D-Q, Dang X-Y, Du A-D, Li D-X, She H-Q (2009) Re-Os
772 dating of pyrite from the Tuolugou stratabound Co(Au) deposit, eastern Kunlun
773 orogenic belt, northwestern China. Ore Geol Reviews 36:213–220
774
775 Finlay AJ, Selby D, Gröcke DR (2010) Tracking the Hirnantian glaciation using Os
776 isotopes. Earth Planet Sci Letters 293:339–348.
777
778 Gabrielse H, Yorath CJ (1989) DNAG #4. The Canadian orogen in Canada. Geosci
779 Canada 16:67–83
780
781 Gadd MG, Layton-Mathews D, Peter JM, Paradis SJ (2016) The world-class Howard's
782 Pass SEDEX Zn-Pb district, Selwyn Basin, Yukon. Part I: trace element
783 compositions of pyrite record input of hydrothermal, diagenetic, and metamorphic
784 fluids to mineralization. Miner Deposita 51:319–342
785

Godwin CI, Sinclair AJ (1982) Average lead isotope growth curves for shale-hosted zinc-lead deposits, Canadian Cordillera. Econ Geol 77:675–690

Goodfellow WD (2004) Geology, genesis and exploration of SEDEX deposits, with emphasis on the Selwyn Basin, Canada. In: Deb M, Goodfellow WD (eds) Sediment-hosted lead-zinc sulphide deposits: attributes and models of some major deposits in India, Australia and Canada. Narosa Publishing House, Delhi, India, pp 24–99

Goodfellow WD, Jonasson IR (1986) Environment of formation of the Howards Pass (XY) Zn-Pb deposit, Selwyn Basin, Yukon. In: Morin JA (ed) Mineral deposits of northern Cordillera. Canad Inst Min Metall Spec Vol 37, pp 19–50

Goodfellow WD, Cecile MP, Leybourne MI (1995) Geochemistry, petrogenesis, and tectonic setting of lower Paleozoic alkalic and potassic volcanic rocks, northern Canadian Cordilleran miogeocline. Canad Jour Earth Sci 32:1236–1254

Goodfellow WD, Lydon JW (2007) Sedimentary exhalative (SEDEX) deposits. In Goodfellow WD (ed) Mineral deposits of Canada: a synthesis of major deposit types, district metallogeny, the evolution of geological provinces, and exploration methods. Geol Assoc Canada, Mineral Deposits Div, Spec Publ 5, pp 163–183

Gordey SP (1980) Stratigraphic cross-section, Selwyn Basin to Mackenzie Platform, Nahanni area, Yukon Territory and District of Mackenzie. In: Current Res, Part A. Geol Survey Canada Paper 81-1A:353–355

Gordey SP, Anderson RG (1993) Evolution of the northern Cordilleran miogeocline, Nahanni map area (1051), Yukon and Northwest Territories. Geol Survey Canada Memoir 428, 214 pp

Gradstein FM, Ogg JG, Schmitz MD, Ogg GM (2012) The geologic time scale 2012. Elsevier, Amsterdam, vol 1-2, 1144 pp

Hnatyshin D, Creaser RA, Wilkinson JJ, Gleeson SA (2015) Re-Os dating of pyrite confirms an early diagenetic onset and extended duration of mineralization in the Irish Zn-Pb ore field. Geology 43:143–146

Hodder R, Bain DJ, Martel E (2014) Interpretive structural geology map and cross-sections of the Howards Pass Zn-Pb district, Yukon and Northwest Territories. Northwest Territories Open File 2014-02, 1 sheet, scale 1:50,000 [includes digital files]

Johnson CA, Slack JF, Falck H, Kelley KD (2014) Depositional environment of mudstone host rocks at the Howards Pass Zn-Pb deposits, Yukon Territory, Canada: insights from iron speciation, sulfur isotopes, and bulk Fe/Al and Mo/TOC ratios: Geol Soc America-Abs Pgms 46(6):250

Jonasson IR, Goodfellow WD (1986) Sedimentary and diagenetic textures, and deformation structures within the sulphide zone of the Howards Pass (XY) Zn-Pb deposit, Yukon and Northwest Territories. In: Morin JA (ed) Mineral deposits of northern Cordillera. Canad Inst Min Metall Spec Vol 37, pp 51–70

Kawasaki K, Symons DTA (2012) Paleomagnetism of the Howards Pass Zn-Pb deposits, Yukon, Canada. Geophys Jour Intern 190:217–229

Kelley KD, Dumoulin JA, Jennings S (2004a) The Anarraaq Zn-Pb-Ag and barite deposit, northern Alaska: evidence for replacement of carbonate by barite and sulfides. Econ Geol 99:1577–1591

Kelley KD, Leach DL, Johnson CA, Clark JL, Fayek M, Slack JF, Anderson VM, Ayuso RA, Ridley WI (2004b) Textural, compositional, and sulfur isotope variations of sulphide minerals in the Red Dog Zn-Pb-Ag deposits, Brooks Range, Alaska: implications for ore formation. Econ Geol 99:1509–1532

Kendall B, Creaser RA, Selby D (2009) ^{187}Re-^{187}Os geochronology of Precambrian organic-rich sedimentary rocks. Geol Soc London Special Publ 326:85–107

Kirby J (2014) Yukon site could be the world's largest undeveloped zinc deposit: Mining & Exploration, http://www.miningandexploration.ca/exploration/article/selwyn_project_represents_one_of_the_largest_undeveloped_zinc_lead_deposits/ (accessed December 2014)

Kirkham G, Dunning J, Schleiss W (2012) Update for Don deposit mineral resource estimate, Howard's Pass property, eastern Yukon: NI 43-101 Technical Rept. Available at: www.sedar.com (accessed June 2014)

Kragh K, Jensen SM, Fougt H (1997) Ore geological studies of the Citronen Fjord zinc deposit, North Greenland: project "Resources of the sedimentary basins of North and East Greenland. Geol Survey Greenland Bull 176:44–49

Large RR, Bull SW, McGoldrick PJ, Walters S, Derrick GM, Carr GR (2005) Stratiform and strata-bound Zn-Pb-Ag deposits in Proterozoic sedimentary basins, northern Australia. In: Hedenquist JW, Thompson JFH, Goldfarb RJ, Richards JP (eds) Econ Geol 100th Anniv Volume, 1905-2005, Soc Economic Geologists, Inc., Littleton, Colo., pp 931–964

Leach DL, Sangster DF, Kelley KD, Large RR, Garven G, Allen CR, Gutzmer J, Walters S (2005) Sediment-hosted lead-zinc deposits: a global perspective. In: Hedenquist JW, Thompson JFH, Goldfarb RJ, Richards JP (eds) Econ Geol 100th Anniv Volume, 1905-2005, Soc Economic Geologists, Inc., Littleton, Colo., pp 561–607

Leach DL, Bradley DC, Huston D, Pisarevsky SA, Taylor RD, Gardoll SJ (2010) Sediment-hosted lead-zinc deposits in Earth history. Econ Geol 105:593–625

Li D, Chen H, Hollings P, Zhang L, Mi M, Li J, Fang J, Wang C, Lu W (2016) Re-Os pyrite geochronology of Zn-Pb mineralization in the giant Caixiashan deposit, NW China. Miner Deposita 51:309–317

Ludwig KR (2003) Isoplot/Ex, version 3: A geochronological toolkit for Microsoft Excel. Berkeley, CA, Geochron Center Berkeley

MacNaughton RB, Fallas KM, Zantvoort W (2008) Qualitative assessment of the Plateau Fault (Mackenzie Mountains, NWT) as a conceptual hydrocarbon play. Geol Survey Canada Open File 5831:1–33

Mair JL, Hart CJR, Stephen JR (2006) Deformation history of the northwestern Selwyn Basin, Yukon, Canada: implications for orogen evolution and mid-Cretaceous magmatism. Geol Soc Amer Bull 118:304–323

Martel E (2015) The structural model for Howard's Pass Zn-Pb district, Northwest Territories: grounds for re-interpretation. Northwest Territories Geol Survey, NWT Open File 2015-01, 54 pp

McClay KR (1991) Deformation of stratiform Zn-Pb (-barite) deposits in the northern Canadian Cordillera. Ore Geol Reviews 6:435–462

McCracken (2014) Paleontological report: report on 37 Ordovician through Late Devonian conodont samples from the Cloudy, Hailstone, Grizzly Bear, Arnica, Tsetso, Marmot, Duo Lake, Nahanni, Mount Kindle, Canol, and unknown formations, District of Mackenzie, NWT collected by Beth Fischer (NTGO). Geol Survey Canada Rept #5-ADM-2013, 25 pp

Morelli RM, Creaser RA, Selby D, Kelley KD, Leach DL, King AR (2004) Re-Os sulphide geochronology of the Red Dog sediment-hosted Zn-Pb-Ag deposit, Brooks Range, Alaska. Econ Geol 99:1569–1576

Morganti JM (1979) The geology and ore deposits of the Howards Pass area, Yukon and Northwest Territories: the origin of basinal sedimentary stratiform sulphide deposits. PhD dissertation, Univ British Columbia, Vancouver, BC, 317 pp

Norford BS, Orchard MJ (1985) Early Silurian age of rocks hosting the lead-zinc mineralization at Howards Pass, Yukon Territory and District of Mackenzie: local biostratigraphy of Road River Formation and Earn Group. Geol Surv Canada Paper 83-18, 35 pp

Nowell GM, Pearson DG, Parman SW, Luguet A, Hanski E (2008) Precise and accurate $^{186}Os/^{188}Os$ and $^{187}Os/^{188}Os$ measurements by multi-collector plasma ionization mass spectrometry, part II: laser ablation and its application to single-grain Pt-Os and Re-Os geochronology. Chem Geol 248:394–426

Peucker-Ehrenbrink B, Ravizza G (2000) The marine osmium isotope record. Terra Nova 12:205–219

Pope MC, Leslie, SA (2013) New data from Late Ordovician-Early Silurian Mount Kindle Formation measured sections, Franklin Mountains and eastern Mackenzie Mountains, Northwest Territories. Geol Surv Canada Current Res 2013-8:1-11

Riediger C, Goodarzi F, MacQueen RW (1989) Graptolites as indicators of regional maturity in lower Paleozoic sediments, Selwyn Basin, Yukon and Northwest Territories, Canada. Canad Jour Earth Sci 26:2003–2015

Schneider J, Melcher F, Brauns M (2007) Concordant ages for the giant Kipushi base metal deposit (DR Congo) from direct Rb-Sr and Re-Os dating of sulphides. Miner Deposita 42:791–797

Scott RJ, Meffre S, Woodhead J, Gilbert SE, Berry RF, Emsbo P (2009) Development of framboidal pyrite during diagenesis, low-grade regional metamorphism, and hydrothermal alteration. Econ Geol 104:1143–1168

Selby D, Creaser RA (2001) Re-Os geochronology and systematics in molybdenite from the Endako porphyry molybdenum deposit, British Columbia, Canada. Econ Geol 96:197–204

Selby D, Creaser RA (2003) Re-Os geochronology of organic rich sediments: an evaluation of organic matter analysis methods. Chem Geol 200:225–240

Selby D, Creaser RA, Stein HJ, Markey R, Hannah JL (2007) Assessment of the 187Re decay constant by cross calibration of the Re-Os molybdenite and U-Pb zircon chronometers in magmatic ore systems. Geochim Cosmochim Acta 71:1999–2013

Selby D, Kelley KD, Hitzman MW, Zieg J (2009) Re-Os sulphide (bornite, chalcopyrite, and pyrite) systematics of the carbonate-hosted copper deposits at Ruby Creek, southern Brooks Range, Alaska. Econ Geol 104:437–444

Selwyn Chihong Mining Ltd., 2016, About the Selwyn Project, SCML Company Fact Sheet. Available at: http://selwynchihong.com/wp-content/uploads/2015/07/SCML_CompanyFactsheet2.pdf

Slack JF, Falck H, Kelley KD, Xue GG (2012) Bottom water redox conditions and sea level changes during Zn-Pb and phosphate mineralization, Howards Pass district, Yukon Territory. Goldschmidt2012 Conference, Montreal, Canada, Mineral Mag 76:2381. Available at: http://www.minersoc.org/goldschmidt-2012/theme.html

Slack JF, Selby D, Dumoulin JA (2015) Hydrothermal, biogenic, and seawater components in metalliferous black shales of the Brooks Range, Alaska: synsedimentary metal enrichment in a carbonate ramp setting. Econ Geol 110:653–675

Smoliar MI, Walker RJ, Morgan JW (1996) Re-Os isotope constraints on the age of Group IIA, IIIA, IVA, and IVB iron meteorites. Science 271: 1099–1102

Snyder DB, Pilkington M, Clowes RM, Cook FA (2009) The underestimated Proterozoic component of the Canadian Cordillera accretionary margin. Geol Soc London Spec Publ 318:257–271

Steele JH, Thorpe SA, Turekian KK (2009) Elements of physical oceanography: a derivative of the encyclopedia of ocean sciences. Academic Press, London, U.K., 660 pp

Tristá-Aguilera D, Barra F, Ruiz J, Morata D, Talavera-Mendoza O, Kojima S, Ferraris F (2006) Re-Os isotope systematics for the Lince-Estefanía deposit: constraints on the timing and source of copper mineralization in a stratabound copper deposit, coastal Cordillera of northern Chile. Miner Deposita 41:99–105

Wilkin RT, Barnes HL (1997) Formation processes of framboidal pyrite. Geochim Cosmochim Acta 61:323–339

Wilkin RT, Arthur MA, Dean WE (1997) History of water-column anoxia in the Black Sea indicated by pyrite framboid size distributions. Earth Planet Sci Lett 148:517–525

Williams N (1978) Studies of the base metal sulfide deposits at McArthur River, Northern Territory, Australia: II. The sulfide-S and organic-C relationships of the concordant deposits and their significance. Econ Geol 73:1036–1056

Zeng, Z, Chen S, Selby D, Yin Z, Wang X (2014) Rhenium-osmium abundance and isotopic compositions of massive sulfides from modern deep-sea hydrothermal systems: implications for vent associated ore forming processes. Earth Planet Sci Letters 396: 223–234

Figures

Fig. 1 Map showing the Mackenzie Platform and time-equivalent shale and chert facies of Selwyn Basin (modified from Goodfellow 2004). Clastic-dominated Zn-Pb (CD Zn-Pb) deposits of Howards Pass district are immediately west of carbonate platform. Other significant Zn-Pb districts of Paleozoic age include Macmillan Pass (Tom and Jason deposits), Anvil (Dy, Faro, Grum, Swim, and Vangorda deposits), and Gataga (Cirque and Driftpile deposits).

Fig. 2 Map showing location of Howards Pass district on border between Yukon and Northwest Territories. At least 15 mineralized centers lie along a northwest-trending belt

termed the "zinc corridor." Samples used for this study were collected from the DON and XY Central (XYC) deposits. SCML, Selwyn Chihong Mining Ltd. Modified from Kirkham et al. (2012).

Fig. 3 Stratigraphic column of Selwyn Basin in Howards Pass district (modified from Morganti 1979; Goodfellow 2004). Howards Pass formation is an informal local name for a ~230-m-thick sequence of mudstone rocks that are stratigraphically equivalent to the Duo Lake Formation of the Road River Group (Morganti 1979). Active member contains all major mineralized zones in Howards Pass district. Deposits in MacMillan Pass and Gataga districts occur in the Devonian Earn Group, whereas those in Anvil district are in lower Cambrian strata (Goodfellow 2004, 2007). Recent mapping by Hodder et al. (2014) reveals complexity of deformation that includes a major flat-lying décollement (red wavy lines) at top of Rabbitkettle Formation, and imbricate thrust faults (grey wavy lines) occurring throughout Duo Lake Formation. Note that Gull Lake and Narchilla Formations are represented, respectively, by Sekwi and Vampire Formations in region (Gordey and Anderson 1993). See text for discussion.

Fig. 4 a Cross section of XYC deposit showing inferred large syncline and relatively uniform thickness of sulphide-bearing zone (active mudstone unit). **b** Cross section of DON deposit illustrating structural disruption, but overall similar stratigraphic sequence compared to other deposits in Howards Pass district (Selwyn Resources, written communication, 2010). Note different scales in **a** compared to **b**.

Fig. 5 Photographs showing textures of pyrite and other sulphides in laminated and layered ore from Howards Pass. **a** Mineralized ore pile sample from the XYC deposit (XYC-txt4; Table 1) consisting primarily of thin (0.05 to 1.5 mm) laminae of sulphides alternating with carbonaceous mudstone, and one relatively thick, crenulated pyrite-rich layer (microscopic textures shown in Fig. 6a, b, and c). Samples used for Re-Os analysis (shown by red arrows) were taken from thick pyrite-rich layer (XYC-txt4(1) and from thinner layer in lower left of photo (XYC-txt4(2); Table 1). **b** Undeformed layered sulphide ore from drill core (sample XYC 116-329; photomicrographs shown in Fig. 6c, d, and e). **c** Pyritic layers in carbonaceous mudstone, contorted and folded (XYC 127-124.5; Table 1); sample for Re-Os is bulk pyrite separate that was not processed into different size fractions. **d** Undeformed interlayered mudstone and sulphides (light layers are sphalerite) showing minor offset (DON 22-68). **e** Pyrite interlayered with mudstone and cut by pressure-solution features (XYC-txt3; Table 1; microscopic textures shown in Fig. 6f). Three portions of rock were processed for Re-Os analysis (shown by red arrows): XYC-txt3(1) from upper right of photograph and XYC-txt3(2) and XYC-txt3(3) from middle and lower portions, respectively; samples were also separated into size fractions (<0.25 mm and 0.25 to 0.5 mm). **f** strongly folded interlayered sulphides and mudstone (DON 137-303.8; photomicrographs shown in Fig. 6g, h, i, j). Core was cut into four equally thick sections and processed for Re-Os analysis; samples were not separated into size fractions. **g** Layered ore (tan layers are sphalerite-rich) from DON deposit, cut by later sulphide-filled cleavages and fractures. **h** Early layered sulphide cut by sulphide-rich shears and mylonitic features.

Fig. 6 Images of pyrite and other sulphides from rocks shown in Figure 5. **a** Photomicrograph in reflected light (rock shown in Fig. 5a) of pyrite framboids in carbonaceous mudstone; note size range of framboids from <10 to 50 μm in diameter. Minor euhedral pyrite grains are also present as overgrowths on framboids or as separate grains. Cross sections of probable pyritized sponge spicules occur in upper portion of photograph. Sphalerite forms subhedral grains in quartz or mudstone matrix among framboids. **b** Backscattered electron (BSE) image of framboidal pyrite (same sample as shown in Fig. 6a); **c** Photomicrograph in reflected light of relatively thick layer of pyrite (Fig. 5a) showing euhedral pyrite in mudstone/quartz matrix. Minor sphalerite and galena (latter not shown) are enclosed in euhedral pyrite. **d** Photomicrograph in reflected light of framboidal pyrite in mudstone with sphalerite; note accumulations of framboidal pyrite form crude layers (dashed lines, rock shown in Fig. 5b). **e** BSE image of sphalerite-rich layer (rock shown in Fig. 5b); sphalerite encloses framboidal and euhedral pyrite and minor galena, within quartz and mudstone matrix. **f** Photomicrograph in reflected light of alternating coarse- and fine-grained layers of pyritic mudstone and minor sphalerite (dashed white lines); solid white lines are direction of superimposed cleavage (rock shown in Fig. 5e). **g** Sphalerite and pyrite in layered ore from the DON deposit (rock shown in Fig. 5f). Darker bands reflect greater proportions of organic matter, but contain pyrite and sphalerite. **h** BSE image showing sphalerite and pyrite from DON deposit (same sample as shown in g), illustrating size range of framboidal pyrite (~2 to 20 μm). **i** Primarily euhedral pyrite intergrown with sphalerite in layered ore from DON deposit (rock shown in Fig. 5f). **j** Photomicrograph in reflected light of pyritized radiolarians with sphalerite from DON deposit. Abbreviations: sp = spicule; sph = sphalerite; gn = galena; py = pyrite.

Fig. 7 $^{187}Re/^{188}Os$ vs. $^{187}Os/^{188}Os$ plots for pyrite separates from DON and XYC deposits. **a** Pyrite from XYC deposit shows limited range in $^{187}Re/^{188}Os$ ratios and more variable $^{187}Os/^{188}Os$ ratios. All Re-Os data lack a geologically or statistically meaningful isochron age. Three separates (open symbols) that did not yield any residue following sample digestion and thus are considered to reflect solely the Re-Os systematics of pyrite, yield an age, although imprecise, which is broadly in agreement with the biostratigraphic age of the host rock (see text). **b** All pyrite separates from the DON deposit lack a geologically meaningful age. However, similar to that shown in (a) for XYC deposit, three separates that did not exhibit residue following digestion (open symbols) yield an age, although highly imprecise, which coincides with that of the host rock (see text for discussion).

Fig. 8 $^{187}Re/^{188}Os$ vs. $^{187}Os/^{188}Os$ plot showing Re-Os data for all pyrite separates from XYC and DON deposits. Linear regression of Re-Os data for pyrite yielding no residue following sample digestion, and therefore having little to no contamination by host rocks (bold red type – open symbols) yields an isochron age of 442 ± 14 Ma (MWSD = 7.4) and initial $^{187}Os/^{188}Os$ value of 0.71 ± 0.07. See text for discussion.

Fig. 9 Approximate biostratigraphic fossil ages for units in Howards Pass district (from Norford and Orchard 1985; McCracken 2014) compared to Re-Os isochron age of pyrite obtained in this study. Biostratigraphic ages from district are shown as black boxes (ruled

or solid for graptolites and conodonts, respectively). Range of ages approximate. Two regional graptolite samples (blue ruled boxes) collected 20 km southwest of Howards Pass (Norford and Orchard 1985), and seven conodont samples (blue solid bars) collected northwest of Howards Pass (blue solid bars) from McCracken (2014) are also shown. See text for discussion.

Table 1. Re-Os data for sulphides from Zn-Pb deposits in the Howards Pass district.

Figure 1

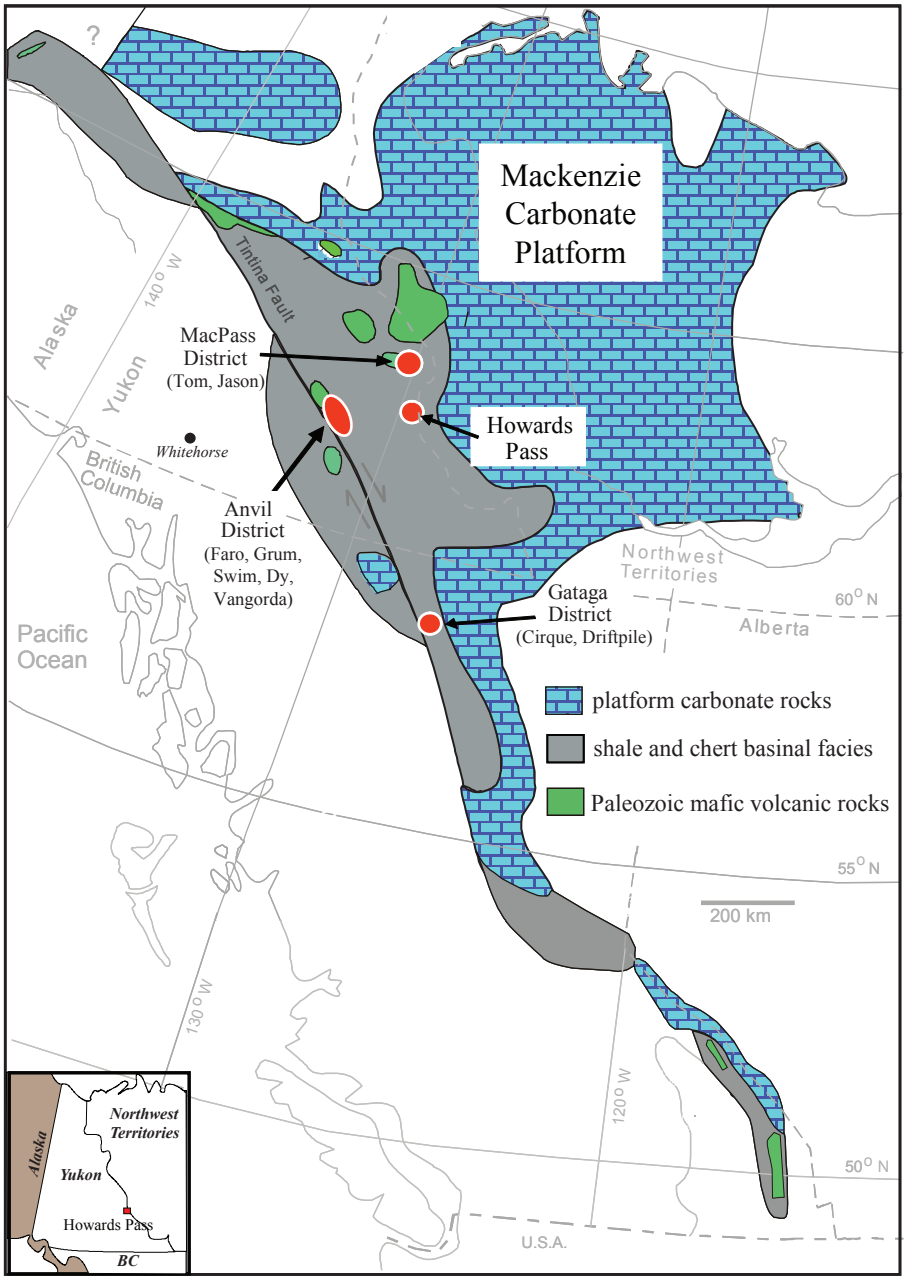

Figure 1.

Figure 2

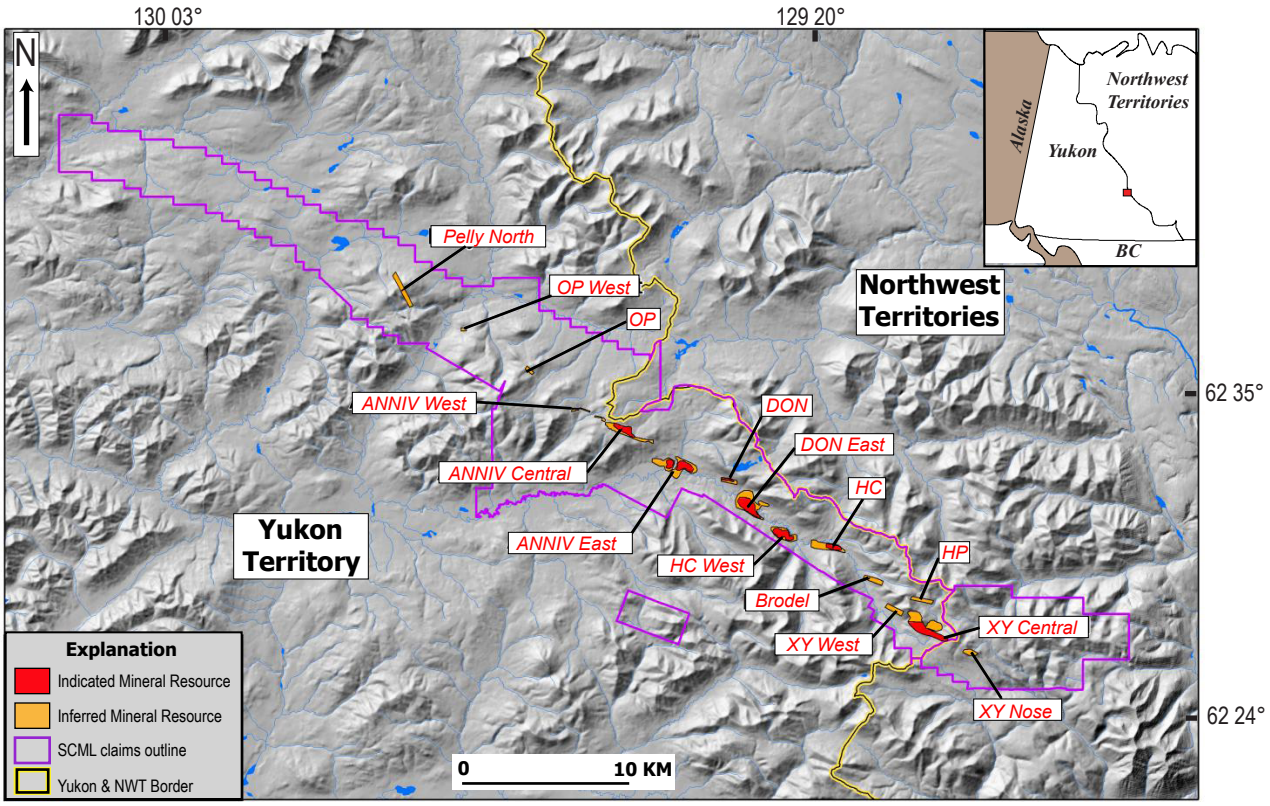

Figure 2.

Figure 3

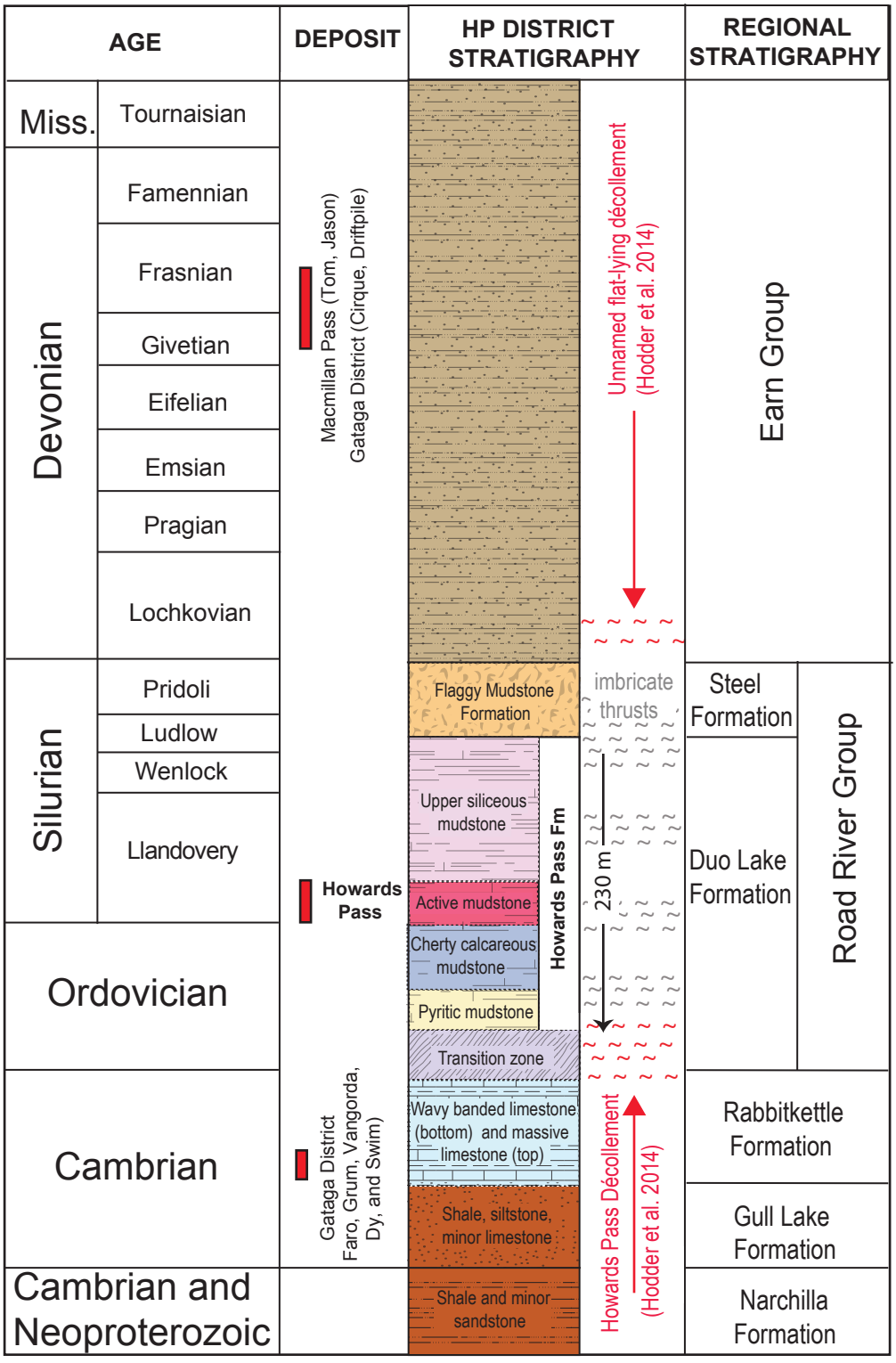

Figure 3.

Figure 4

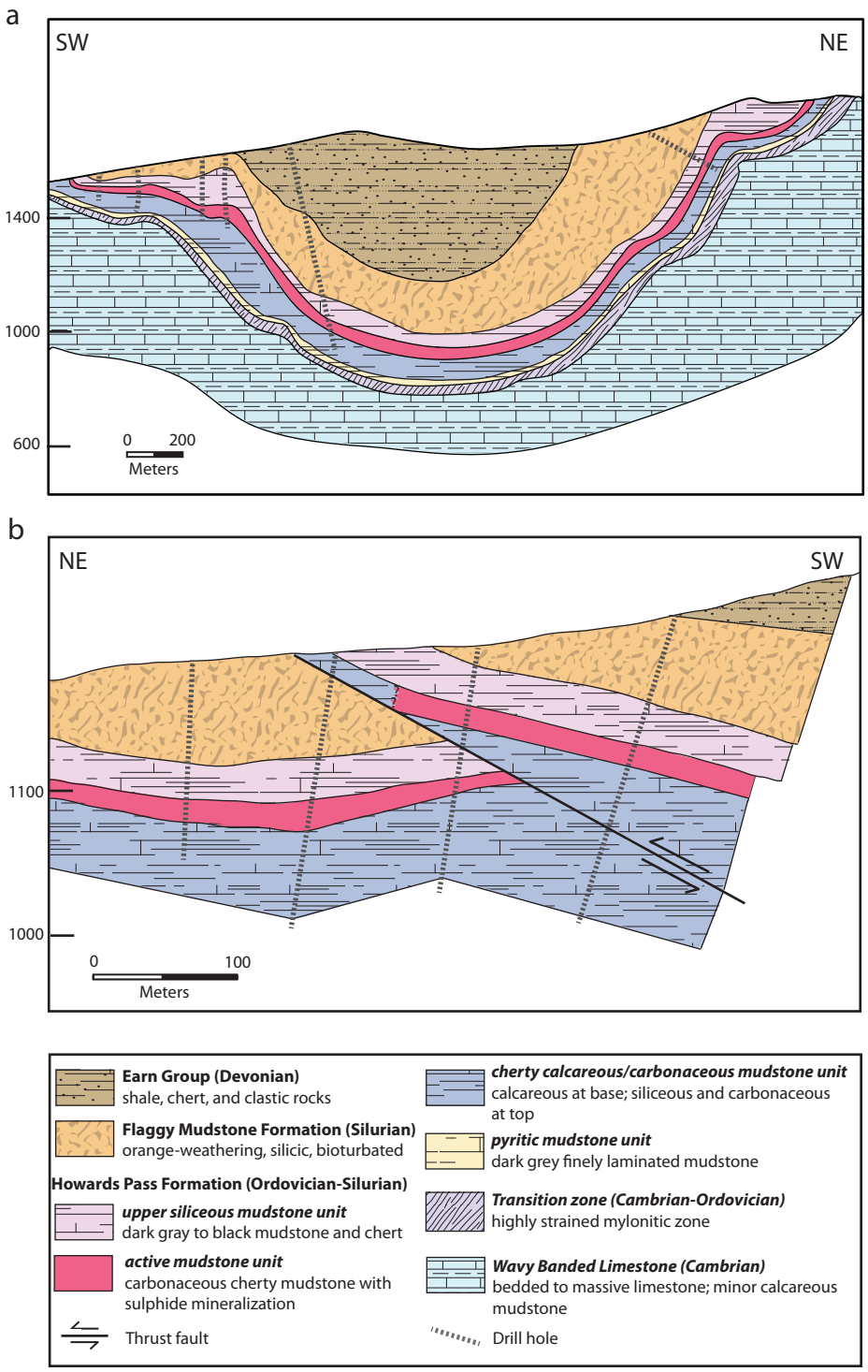

Figure 4.

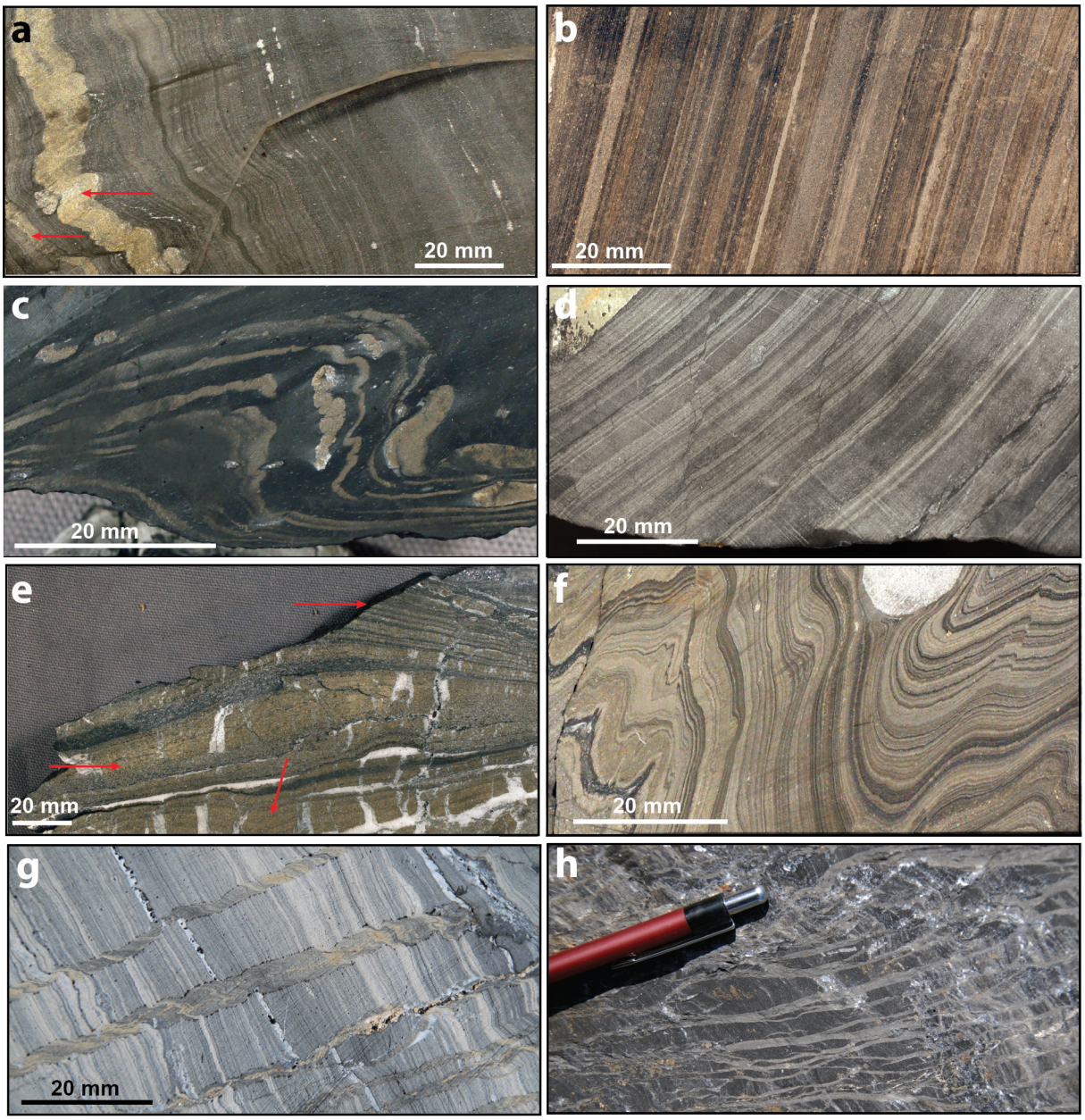

Figure 5.

Figure 6

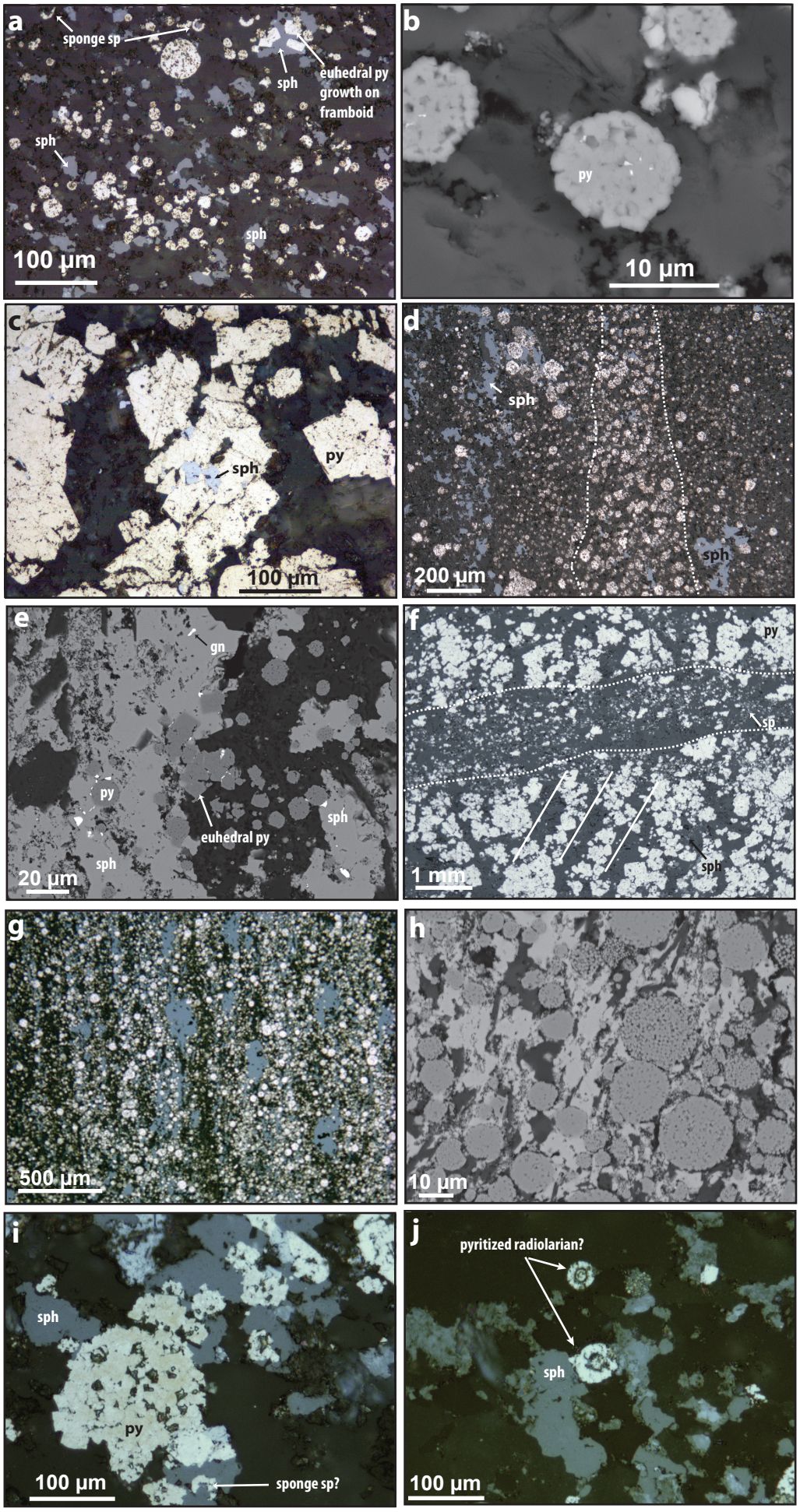

Figure 6.

Figure 7

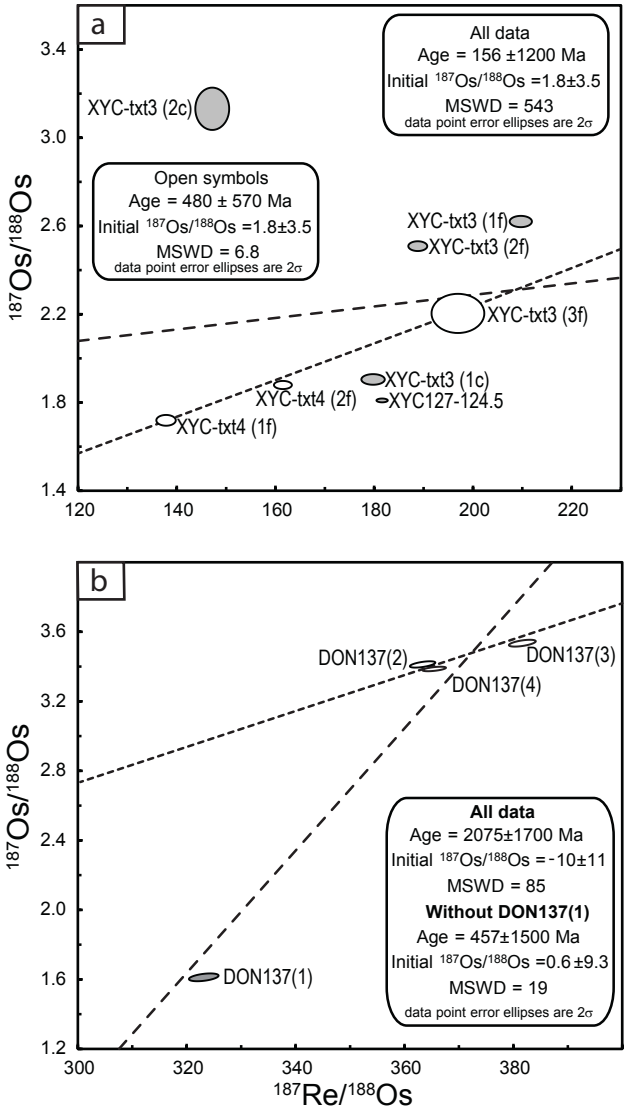

Figure 7.

Figure 8

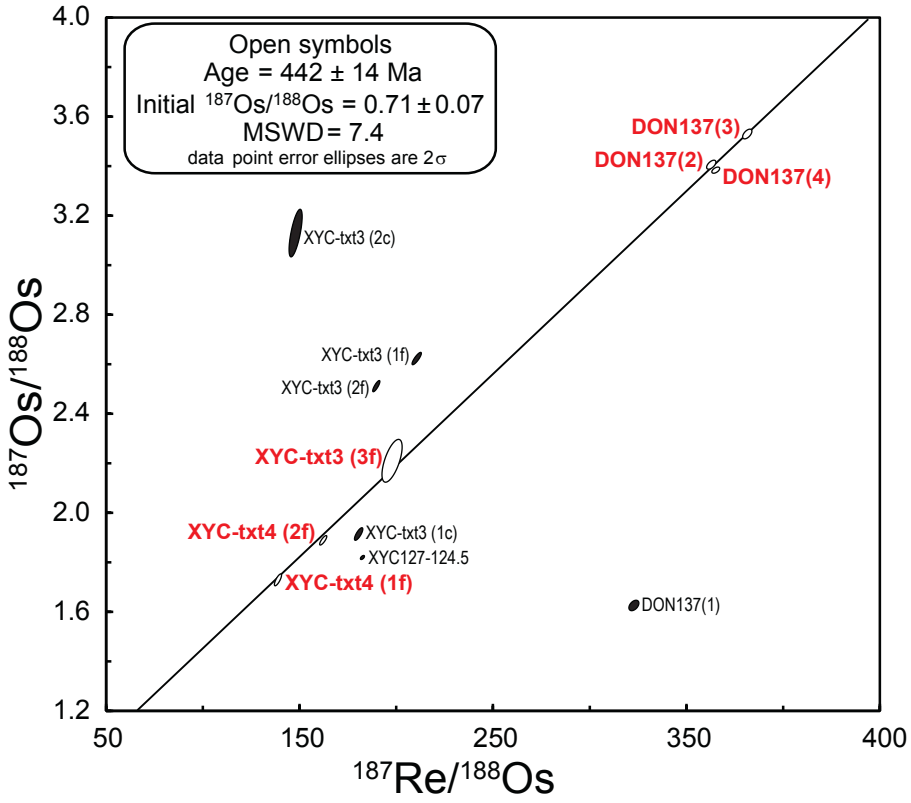

Figure 8.

Figure 9

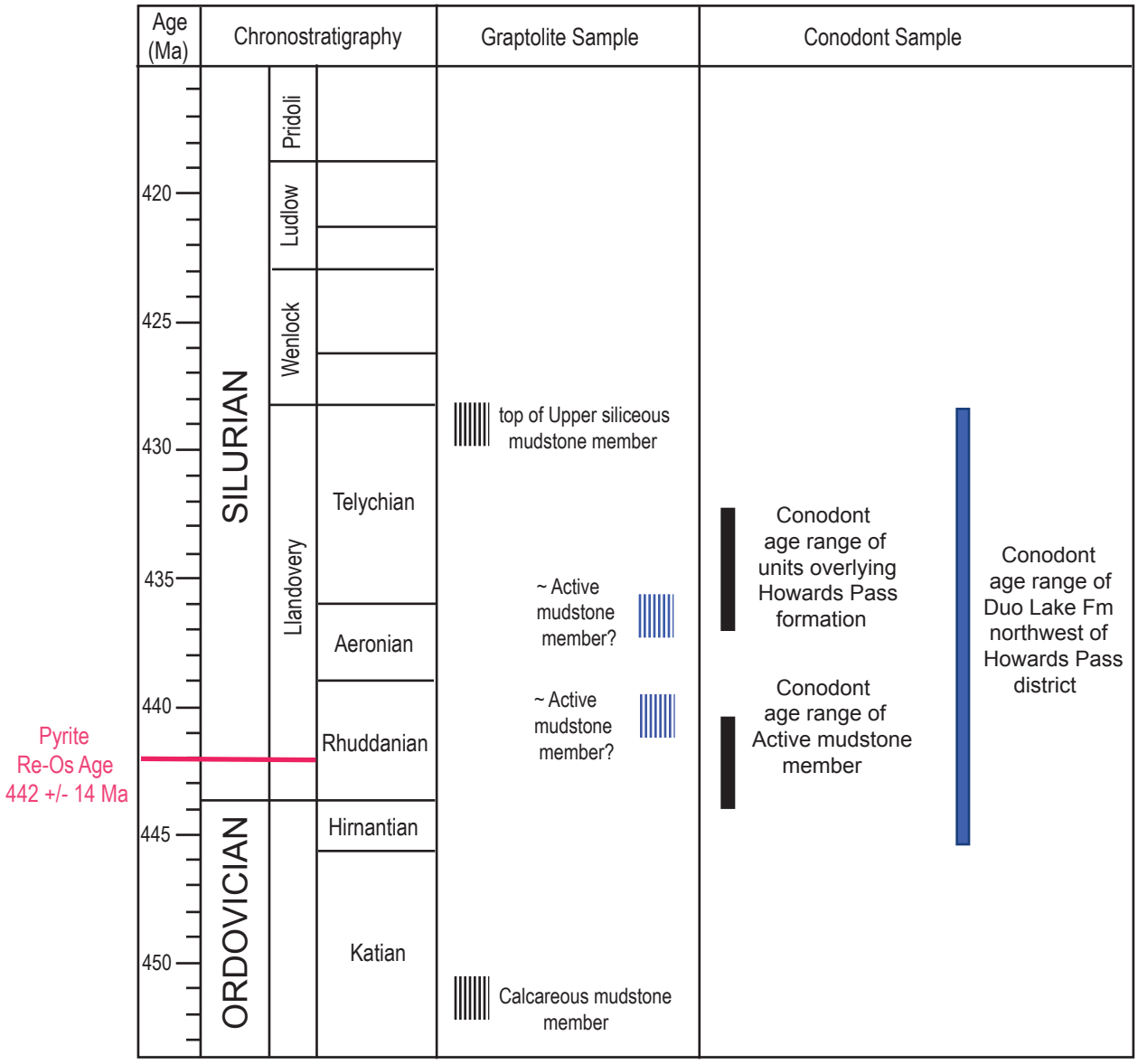

Figure 9.

Table

Sample number	Sample Type[a]	size fraction	Post digestion residue[b]	Re (ppb)	±[c]	Os (ppt)	±[c]	^{192}Os (ppt)	±[c]	^{187}Re/^{188}Os	±[c]	^{187}Os/^{188}Os	±[c]	rho[d]	Osi @ 442
XYC deposit															
Sample 1 - 5 sub samples															
XYC-txt3 (1c)	pyrite+HR	~0.25 to 0.5 mm	*yes - minor*	5.36	0.03	177.1	0.8	59.3	0.5	179.7	1.9	1.908	0.020	0.780	0.58
XYC-txt3 (1f)	pyrite+HR	<0.25 mm	*yes*	5.39	0.02	164.1	0.6	51.1	0.4	209.7	1.8	2.619	0.020	0.847	1.07
XYC-txt3 (2c)	pyrite+HR	~0.25 to 0.5 mm	*yes*	3.70	0.02	169.0	1.8	50.1	0.9	146.9	2.8	3.128	0.078	0.693	2.04
XYC-txt3 (2f)	pyrite+HR	<0.25 mm	*yes*	3.86	0.02	129.0	0.4	40.6	0.3	188.8	1.6	2.508	0.018	0.832	1.11
XYC-txt3 (3f)	pyrite[f]	<0.25 mm	*no*	3.97	0.02	123.4	1.4	40.1	0.9	197.0	4.4	2.205	0.071	0.644	0.75
Sample 2															
XYC-txt4 (1f)	pyrite[f]	<0.25 mm	*no*	2.21	0.01	93.4	0.4	31.9	0.3	137.6	1.6	1.723	0.019	0.782	0.71
XYC-txt4 (2f)	pyrite[f]	<0.25 mm	*no*	3.34	0.02	122.6	0.4	41.2	0.3	161.3	1.5	1.883	0.015	0.815	0.69
Sample 3															
XYC127-124.5	pyrite+HR	<0.5 mm	*yes - minor*	21.38	0.08	692.3	1.0	234.3	0.8	181.6	0.9	1.813	0.007	0.580	0.47
DON deposit															
Sample 4 - 4 subsamples (same core interval separated into 4 equal parts)															
DON137(1)	pyrite+HR	<0.5 mm	*yes*	33.65	0.13	599.8	1.9	207.3	1.2	322.9	2.3	1.618	0.018	0.441	-0.77
DON137(3)	pyrite[f]	<0.5 mm	*no*	34.94	0.13	636.8	1.4	182.1	0.7	381.7	2.0	3.530	0.016	0.566	0.71
DON137(4)	pyrite[f]	<0.5 mm	*no*	36.99	0.14	694.9	1.1	201.4	0.6	365.4	1.7	3.382	0.011	0.546	0.68
DON137(2)	pyrite[f]	<0.5 mm	*no*	34.04	0.13	644.8	1.4	186.5	0.7	363.1	1.9	3.403	0.015	0.580	0.72
DON111-157.8	fresh mudstone	powdered		50.85	0.17	1632.2	5.3	514.4	0.9	196.7	0.7	2.505	0.005	0.345	1.05

[a]HR = host rock (Active mudstone member, Howards Pass formation)

[b]Mineral separates of 6 samples contained a significant residue (silicate minerals including quartz, muscovite, clays) after dissolution of the sample in *aqua regia* acid, interpreted to be the un portion of the host rock. However, organic matter present as fine intergrowths with, or contained within pyrite, or as coatings on grains is dissolved in *aqua regia;* hence, the resulting Re-Os d represents a mix of Re and Os liberated from both pyrite and organic matter.

[c]Uncertainties reported at the 2 sigma level. ^{187}Os/^{188}Os uncertainites reported at 2s.d.